Near-Infrared Raman Spectroscopy Using a Diode Laser and CCD Detector for Tissue Diagnostics

Diploma Paper
by
Ulf Gustafsson

Lund Reports on Atomic Physics, LRAP-138
Lund, September 1993

1. Abstract

This paper surveys the possibility to observe high-quality NIR Raman spectra of both fluorescent and non-fluorescent samples with the use of a diode laser, a fibre optic sampler, a single spectrometer and a charge-coupled device (CCD) detector. A shifted excitation difference technique was implemented for removing the broad-band fluorescence emission from Raman spectra of the highly fluorescent samples. Raman spectra of 1,4-dioxane, toluene, rhodamine 6G, and HITCI in the 640 to 1840 cm^{-1} spectral region and 1,4-dioxane and toluene in the 400 to 3400 cm^{-1} spectral region have been recorded.

The results open the field of sensitive tissue characterisation and the possibility of optical biopsy *in vivo* by using NIR Raman spectroscopy with fibre optic sampling, a single spectrometer, and a CCD detector.

Contents

2 Introduction and theory

2.1 Introduction

In the practise of medicine the physician is confronted by the two major aspects of clinical problem solving, diagnostics and therapeutics. The outcome of the diagnostic process is the key to the answer and outcome of the therapeutic process. Sensitive methods and techniques for discriminating between healthy and diseased tissue are often needed in the diagnostic process. Often an early diagnosis is of great importance for the prognosis and the treatment of the disease. In certain cases it may also be desirable to begin a treatment at the same time as the diagnose is set, but techniques that utilise this approach are more or less still in its infancy.

The ultimate and often indispensable method in tissue diagnostics is conventional biopsy, i.e. to remove a small amount of tissue (and/or fluid) from the living body and to examine it to establish the assumed presence of disease. Biopsy provides outstanding histochemical information of tissue. However, in some cases it is difficult or impossible to remove even a small amount of tissue for examination. Biopsy is also often guided by naked-eye inspection and it may be difficult to distinguish between healthy and diseased tissue just by the look of it. If the physician only suspects a disease, then the number of biopsy samples will probably exceed the manageable.

In these cases, sensitive techniques that utilise new approaches for medical diagnosis, such as optical spectroscopy, would be of great value. In all spectroscopic techniques there is a mechanism by which the incident radiation, the light, interacts with the molecular energy levels of the investigated matter. The light may be transmitted, absorbed, or scattered and therefore it is not surprising that several spectroscopic techniques for tissue characterisation have been developed over the last decade. Light delivered and collected via for instance flexible optical fibres provides access to many organs in the body and can be used both in the diagnostic process and as a guidance system in for instance surgical laser applications.

The running description in this paper assumes at least some basic knowledge of the units as well as their internal relations involved in atomic and molecular spectroscopy. For those who are not familiar with them a brief description is given in Appendix A.

2.2 Spectroscopic techniques for tissue characterisation

Laser-induced fluorescence. The most commonly used and known technique for diagnosis of diseased tissue is laser induced fluorescence (LIF). In LIF laser light excites the atoms and molecules to higher electronic states and the fluorescence emission that is released in the subsequent decay is observed. LIF relies on the fact that different types of tissue is characterised by different spectral or temporal signatures, thus enabling to discriminate between diseased and healthy tissue by analysing the fluorescence signal. Spectrally resolved LIF is still under development for a wide range

of clinical applications, e.g. in the diagnosis and therapy (photodymanic therapy, PDT) of malignant tumours [1,2], in the diagnosis and treatment (laser angioplasty) of atherosclerosis in blood vessels [1,3,4], in the characterisation of human kidney stones and ureter tissue [5,6], and in studies of caries teeth [7,8].

Time-resolved laser-induced fluorescence. Since fluorescence spectra from tissue are rather broad and structureless another fluorescence emission technique known as time-resolved LIF is also being used. The time-resolved LIF can be seen as a complement to ordinary LIF and gives valuable additional information. In time-resolved LIF it is the temporal behaviour of the fluorescence decay that is observed and the difference in fluorescence decay curves allows the discrimination between healthy and diseased tissue. The technique, which frequently uses picosecond (10^{-12} second) spectroscopy since the lifetimes involved are normally short, has been used in studies of e.g. atherosclerosis [9,10] and for tumour demarcation [10].

Transillumination. Another interesting optical spectroscopic technique is transillumination. This method uses visible light, often from a laser, and is based on the characteristic attenuation of light in turbid media, such as tissue. In the visible and near-infrared (NIR) region scattering is more likely to occur than absorption. In order to measure absorption and scattering separately and to improve spatial resolution time-resolved transillumination techniques are often being used. The light that leaves the tissue first, has travelled the shortest distance within the tissue. Thus, the intensity of this early light will depend on the optical properties of a volume close to a straight line through the tissue and contains more information about the spatial localisation of different optical properties. The time-resolved transillumination technique is relatively new in tissue characterisation and is in development for breast tumour detection [11,12].

Infrared spectroscopy. Infrared (IR) spectroscopy uses, as the name indicates, an infrared light source to probe the vibrational or rotational energy levels of molecules. The term IR spectroscopy refers both to IR absorption spectroscopy (mostly used for gases and liquids) and to IR reflection spectroscopy (mostly used for solids). What differs IR spectroscopy and the above described techniques is that it uses a continuum or polychromatic light source which is usually some solid material heated to incandescence by an electric current. IR spectroscopy, especially in the near-infrared (NIR) region, has been and is still being used in a wide variety of applications [13,14] but its applications in tissue characterisation has to my knowledge so far been limited to the analysis of the arteries and atherosclerosis [15,16].

Raman scattering. A technique that is closely related to IR spectroscopy, as it also probes the vibrational or rotational energy levels of molecules, is Raman scattering. Raman scattering is an inelastic light-scattering effect, where, like in the case of laser-induced fluorescence, a wavelength change occurs in the process of light interaction with matter. Raman scattering uses, as it is carried out today, a laser exclusively as the light source. A Raman spectrum (like an IR spectrum) reflects the disposition of atomic nuclei and chemical bonds within a molecule and the interactions between the molecule and its immediate environment, and can thus be used as a monitor of molecular chemistry.

Even if IR and Raman spectra both involve vibrational and rotational energy levels they are not duplicates but complements to each other. Much of the information

contained in a Raman spectrum does not appear in the IR spectrum and vice versa. Some vibrations or rotations of molecules may appear in the IR spectrum only, some in the Raman spectrum only and some in both or in neither. The widespread use of Raman spectroscopy in biological systems has been driven by the fact that most Raman spectra are obtained in the visible region of the electromagnetic spectrum and that water (which to some degree is always present in biological systems or biochemical solutions) is an exceptionally weak Raman scatterer but an exceptionally strong IR absorber.

Compared with for instance laser-induced fluorescence, Raman scattering provides much more information about a tissue sample, since sharp spectral lines result rather than broad fluorescence features. This is a consequence of the processes involved and another reason of the interest in Raman spectroscopy.

Since the biological applications (and other applications also) of Raman spectroscopy seems to have some rather interesting features I have chosen to evaluate its potential in tissue characterisation, especially atherosclerosis.

2.3 Theory of Raman scattering

2.3.1 Introduction

In 1928 the Indian scientist C.V. Raman, with the help of K.S. Krishnan, observed an effect that at first was called "feeble fluorescence" and later "New Radiation" [17,18,19]. The importance of the discovery was recognised in 1930 when Raman was awarded by the Nobel Prize in Physics and the discovery is known as Raman scattering, the Raman effect, or Raman spectroscopy ever since.

Raman scattering is one form of a wide variety of light-scattering phenomena and occurs if the scattering particles are small compared to the wavelength of the light. In Raman scattering a change in wavelength occurs and is therefore referred to as an *inelastic* light-scattering effect. If the scattered light instead has the same wavelength as the incident light, *elastic* Rayleigh scattering has occurred. The probability for these scattering phenomena are strongly dependent on the wavelength and, which will be shown later, are proportional to λ^{-4}.

Another form of light-scattering may also occur. If the scattering particles (smoke or fog, for example) are considerable larger than the wavelength of the light an *elastic* form if scattering, named Mie scattering, occurs. The probability for Mie scattering is a complicated function of wavelength, particle radius, refractive indices, and absorption. The intensity of the scattered light is approximately proportional to λ^{-2}, i.e. it increases towards shorter wavelengths.

Raman scattering is the result of the interaction between the incident light and the vibrational or rotational energy levels of molecules, but in the biochemical context, Raman spectroscopy is concerned primarily with those wavelength changes, or for that matter frequency changes, that occur as a result of the coupling between the incident radiation and the vibrational energy levels of molecules. Consequently, the Raman spectrum is a vibrational spectrum of a molecule.

Raman scattering can be described with both classical physics and quantum mechanics, and both descriptions have their advantages and drawbacks. The classical

approach provides a useful conceptual model for Raman scattering, and the quantum mechanical approach provides valuable information about e.g. intensities and polarisation properties of Raman scattering. The representation given here has the intention of providing a sufficient understanding of the essential nature of Raman scattering. A more extensive and detailed description of Raman theory is given in for instance the book by Long [20].

2.3.2 A classical model for Raman scattering

A light wave is a travelling electromagnetic wave of which only the electric component produces Raman scattering. Suppose that the electric field associated with the light is represented by

$$\mathrm{E} = E_0 \cos 2\pi\nu t \tag{2.1}$$

where E_0 is the maximum, and ν the frequency. When the light wave meets a molecule it tends to displace the electrons from their average position around the positively charged nuclei. The displacements result in an induced dipole moment P in the molecule, such that

$$\mathrm{P} = \alpha\mathrm{E} = \alpha E_0 \cos 2\pi\nu t \tag{2.2}$$

where the proportionality constant α is called the polarisability. In general, P is not directed along E and α is replaced by a polarisation tensor α. The expression for P can be rewritten in terms of Cartesian components

$$\begin{aligned} P_x &= \alpha_{xx}E_x + \alpha_{xy}E_y + \alpha_{xz}E_z \\ P_y &= \alpha_{yx}E_x + \alpha_{yy}E_y + \alpha_{yz}E_z \\ P_z &= \alpha_{zx}E_x + \alpha_{zy}E_y + \alpha_{zz}E_z \end{aligned} \tag{2.3}$$

and this can be expressed as a matrix equation $\mathrm{P} = \alpha\mathrm{E}$, that is

$$\begin{bmatrix} P_x \\ P_y \\ P_z \end{bmatrix} = \begin{bmatrix} \alpha_{xx} & \alpha_{xy} & \alpha_{xz} \\ \alpha_{yx} & \alpha_{yy} & \alpha_{yz} \\ \alpha_{zx} & \alpha_{zy} & \alpha_{zz} \end{bmatrix} \begin{bmatrix} E_x \\ E_y \\ E_z \end{bmatrix} \tag{2.4}$$

and hence, α is said to be a tensor. For almost every case, α is a symmetric matrix ($\alpha_{xy} = \alpha_{yx}, \ldots$).

If a molecule vibrates, its polarisability varies. The vibrational modes (displacements) Q of the molecule can be described as

$$Q = Q_0 \cos 2\pi\nu_{vib} t \tag{2.5}$$

where Q_0 is the maximum displacement measured from equilibrium configuration, and ν_{vib} is the vibration frequency. For small vibrations, the polarisability can be written

(expanded in a Taylor series) as

$$\alpha = \alpha_0 + \left(\frac{\partial \alpha}{\partial Q}\right) Q + \ldots (\text{higher order terms}). \tag{2.6}$$

Combining Eqs. (2.5) and (2.6)

$$\alpha = \alpha_0 + \left(\frac{\partial \alpha}{\partial Q}\right) Q_0 \cos 2\pi \nu_{vib} t. \tag{2.7}$$

The substitution of this value for α into Eq. (2.2) yields

$$\mathrm{P} = \alpha_0 E_0 \cos 2\pi \nu t + \left(\frac{\partial \alpha}{\partial Q}\right) \frac{Q_0 E_0}{2} \cos 2\pi \nu t \cos 2\pi \nu_{vib} t. \tag{2.8}$$

Making use of the trigonometric identity, $\cos\theta \cos\varphi = \cos(\theta + \varphi) + \cos(\theta - \varphi)$, we can write

$$\mathrm{P} = \alpha_0 E_0 \cos 2\pi \nu t + \left(\frac{\partial \alpha}{\partial Q}\right) \frac{Q_0 E_0}{2} \left(\cos 2\pi (\nu + \nu_{vib}) t + \cos 2\pi (\nu - \nu_{vib}) t\right). \tag{2.9}$$

Eq. (2.9) demonstrates the three major components in a Raman scattering experiment. The first term, known as *Rayleigh scattering*, is elastic, i.e. the scattered light has the same frequency as the incident light. The second and the third terms are inelastic scattering, i.e. the frequency of the scattered light is shifted up or down in relation to the frequency of the incident light. The up-shifted component, vibrating at a frequency equal to the sum of the frequencies of the light and the molecular vibration, is called *anti-Stokes Raman scattering*. The down-shifted component, vibrating at a frequency given by that of the light wave minus that of the molecule, is known as *Stokes Raman scattering*.

Thus, when a light beam interacts with some material it will be scattered with frequencies:

ν = Rayleigh scattering

or

$\nu \pm \nu_{vib}$ = Raman scattering.

Eq. 2.9 also shows that for Raman scattering to occur,

$$\frac{\partial \alpha}{\partial Q} \neq 0 \tag{2.10}$$

i.e., a vibration is said to be Raman active if the polarisability of the molecule changes during a vibration.

2.3.3 A quantum mechanical picture of Raman scattering

In the quantum mechanical approach to Raman scattering the quantisation of molecular energy levels are taken into account. Consider a vibrating molecule and suppose that it is represented by a harmonic oscillator. The vibrational energy E_{vib} of the ground state of this molecule is

$$E_{vib} = (n+\tfrac{1}{2})h\nu_{vib} \tag{2.11}$$

where h is Plank's constant, ν_{vib} is the vibrational ground frequency, and n is the vibrational quantum number controlling the energy of that particular vibration and it has values of 0, 1, 2, 3, ... etc. The vibrational energy levels in the ground state are thus equally spaced, quantified, by the amount ν_{vib}. In the quantum mechanical model, light scattering is depicted as a two-photon process. The first step is the interaction between a photon of frequency ν and a molecule which raise the molecule to a higher energy state. The second step involves the release of another photon and the relaxation of the molecule.

For *Rayleigh scattering* the transitions have, apart from a change in sign, the same energies and thus no change in frequency of the photon occurs. For *Stokes scattering* the lowering transition stops on a vibrational energy level that is higher than the starting level, and this photon has a frequency $\nu-\nu_{vib}$. If the second transition stops on a vibrational energy level lower than the starting level, a photon with a frequency $\nu+\nu_{vib}$ is released, and *anti-Stokes scattering* has occurred. Naturally, the total energy is conserved in the transitions, and for Stokes scattering the molecule gain an energy $h\nu_{vib}$ while for anti-Stokes scattering the reverse is true.

For Raman spectroscopy, as it is usually practised, the higher energy levels are not located in an upper (excited) electronic state of the molecule. Instead, virtual levels are introduced, and therefore there are no lifetimes associated with Raman scattering. Raman scattering is thus an instant effect. Fig. 2.1 shows the processes in a Raman scattering experiment.

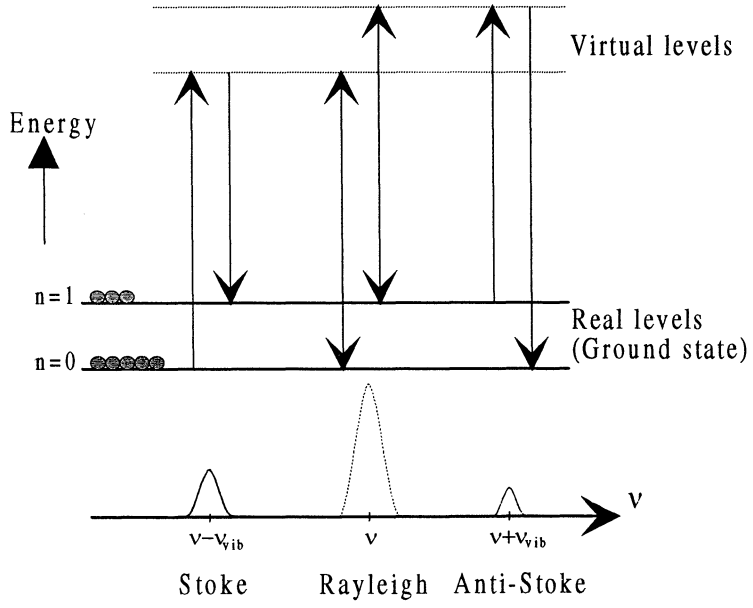

Fig. 2.1 *Rayleigh and Raman Scattering.*

2.3.4 Raman intensities

Classical theory gives the average rate of total radiation I from an oscillating dipole

$$I = \frac{2}{3c^2}\overline{\left(\frac{\partial^2 \mathrm{P}}{\partial t^2}\right)^2} \tag{2.12}$$

where the bar denotes time averaging, and c is the speed of light. Inserting the Rayleigh, Stokes and Anti-Stokes components from Eq. (2.9) yield

$$I_{Rayleigh} = K_R \nu^4 I_0 {\alpha_0}^4 \tag{2.13}$$

$$I_{Stokes} = K(\nu - \nu_{vib})^4 I_0 \left(\frac{\partial \alpha}{\partial Q}\right)^2 \tag{2.14}$$

$$I_{anti-Stokes} = K(\nu + \nu_{vib})^4 I_0 \left(\frac{\partial \alpha}{\partial Q}\right)^2 \tag{2.15}$$

where K_R and K are constants (that summarise some other rather uninteresting constants), and I_0 is the incident light intensity.

As can be seen from Eqs. (2.14) and (2.15) the intensity of Raman light is proportional to the forth power of the scattered light. This is the so-called ν^4 law and demonstrates that the Raman scattered light strongly decreases with diminishing values of ν, or put differently, the Raman intensity strongly increases with diminishing values of λ.

The relative intensities of the Stokes and the anti-Stokes components are only predicted to differ by the ratio of $\left[(\nu - \nu_{vib})/(\nu + \nu_{vib})\right]^4$ which is not consistent with experiment. If a full quantum mechanical treatment is carried out, the ratio of the Stokes and the anti-Stokes intensities becomes

$$\frac{I_{Stokes}}{I_{anti-Stokes}} = \frac{(\nu - \nu_{vib})^4}{(\nu + \nu_{vib})^4} \exp(h\nu_{vib}/kT) \tag{2.16}$$

where h is Plank's constant, k is Boltzmann's constant, and T is the absolute temperature. The expression is verified experimentally at thermal equilibrium, and is actually quite plausible. The ratio of the number of molecules (N) in two vibrational energy levels is governed by the Boltzmann distribution,

$$N_{upper}/N_{lower} = exp(h\nu_{vib}/kT). \tag{2.17}$$

Referring to Fig. 2.1, anti-Stoke scattering starts in an *upper* vibrational state and Stokes scattering starts in a *lower* state. Combine Eq.(2. 17) and $\left[(\nu - \nu_{vib})/(\nu + \nu_{vib})\right]^4$, and we end up with Eq.(2.16).

When the vibrational frequency is ν_{vib}= 400 cm^{-1} (corresponds to a vibrational energy splitting of ≈ 0.05 eV), the temperature is 300 K, and incident light frequency is

ν = 12500 cm^{-1} (corresponds to λ = 800 nm), $I_{anti-Stokes} = 0.2 I_{Stokes}$. Changing the vibrational frequency to ν_{vib} = 2000 cm^{-1} yields $I_{anti-Stokes} = 0.0002 I_{Stokes}$. Therefore, anti-Stokes scattering is weak and usually ignored in normal Raman spectroscopy. The Raman spectrum of carbontetrachloride in Fig. 2.2 clearly shows the intensity difference between Stokes and anti-Stokes scattering.

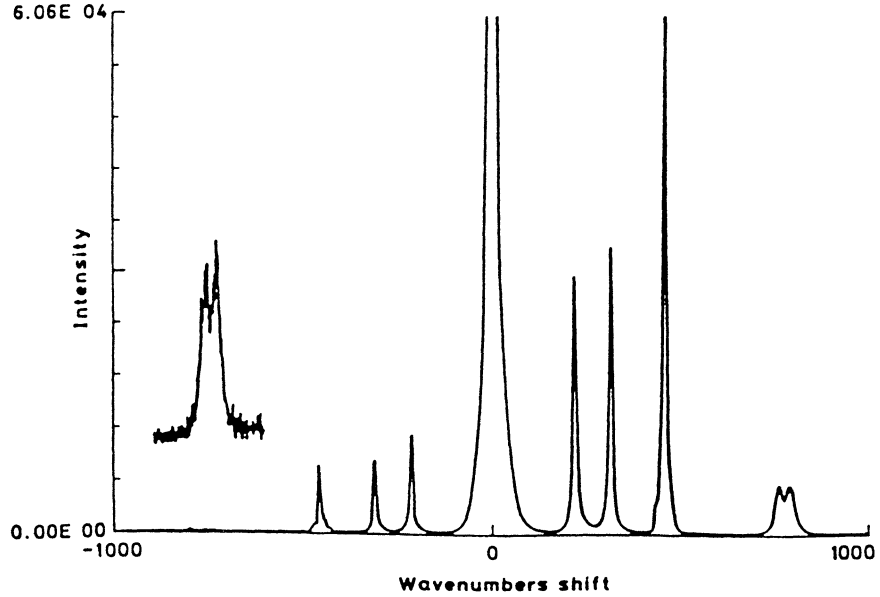

Fig. 2.2 *Stokes and anti-Stokes spectrum of carbontetrachloride (CCl_4). The anti-Stokes band at ≈ -790 cm^{-1} has been magnified by X100. (From Ref. [22].)*

The relative intensities of incident light, Rayleigh scattering and Raman scattering would have been easy to calculate if it were not for the unknown values of α_0 and $\partial\alpha/\partial Q$. The quantum mechanical approach provides the means of calculating the different polarisabilities, but this will not be done here. It is expected that $\partial\alpha/\partial Q$ will be much smaller than α_0, and this is in fact the case. Approximately, the following relationships hold:

$$I_{Raman} = 10^{-5} - 10^{-3} I_{Rayleigh} = 10^{-8} - 10^{-6} I_{Incident}$$

2.3.5 Other Raman scattering effects

Resonance Raman effect. In the quantum mechanical treatment the factor $\partial\alpha/\partial Q$ is replaced by the transition polarisation tensor $(\alpha_{ij})_{mn}$, which can be derived using time dependent perturbation theory. The total intensity of the Raman scattered light resulting from a molecular transition between state *m* and *n* thus becomes (cf. Eqs. (2.14) and (2.15))

$$I = K(\nu_0 + \nu_{mn})^4 I_0 \sum_{ij} \left| (\alpha_{ij})_{mn} \right|^2 \qquad (2.18)$$

where

$$(\alpha_{ij})_{mn} = \frac{1}{h}\sum_r \frac{\langle n|\mu_j|r\rangle\langle r|\mu_i|m\rangle}{\nu_{rm} - \nu_0 + i\Gamma_r} + \frac{\langle n|\mu_i|r\rangle\langle r|\mu_j|m\rangle}{\nu_{rn} + \nu_0 + i\Gamma_r}. \quad (2.19)$$

The molecule is perturbed by light of frequency ν_0 and intensity I_0, causing a transition from state m to n and scattered light of frequency $\nu_0 \pm \nu_{mn}$. Index r covers all the eigenstates of the molecule, h is Plank's constant, Γ_y is a damping constant, and $\langle n|\mu_j|r\rangle$, etc., are the amplitudes of the electric dipole transition moments, where μ_j is the electric dipole moment operator along direction j.

If ν_0 approaches an allowed molecular transition ν_{rm}, $(\nu_{rm} - \nu_0 + i\Gamma_r)$ becomes small, i.e. one term in the sum becomes very large. These terms dominate the Raman scattering, and observed spectra change dramatically. It is a resonance condition, and the phenomenon is known as *resonance Raman scattering* or *resonance Raman effect.*

It is important to notice that all of the expressions derived in the previous chapters are only valid if ν_0 is far from any allowed molecular transition ν_{rm}, but in conventional Raman spectroscopy this is always the case, which justifies their use (and they are indeed a bit simpler than Eqs. (2.18) and (2.19)!).

Non-linear Raman effects. The induced dipole moment was given by Eq. (2.2), $P = \alpha E$, but actually this is a simplification. The induced dipole moment is in fact a series of terms given by

$$P = \alpha E + \beta EE + \gamma EEE + \ldots \quad (2.20)$$

where α is the polarisability, β is the hyperpolarisability, and γ is the second hyperpolarisability. These terms are responsible for a number of effects known as *non-linear Raman scattering*. The components typically decrease by ten orders of magnitude for each higher-order term in the equation.

According to the quantum mechanical theory for the harmonic oscillator potential the only allowed change in the vibrational quantum number for a Raman transition is

$$\Delta n = \pm 1 \quad (2.21)$$

To explain the non-linear Raman effects an expansion of the harmonic potential to a more realistic anharmonic is carried out. In the anharmonic potential other changes ("overtones") in the vibrational quantum number are also allowed, such as

$$\Delta n = \pm 1, \pm 2, \pm 3, \ldots \quad (2.22)$$

but also "combined overtones" is allowed, i.e. two or more different vibrational ground frequencies may be involved (as $\nu_{vib1} \pm \nu_{vib2}$ and $2\nu_{vib1} \pm \nu_{vib2}$).

Fig. 2.3 contrasts normal Raman scattering, hyper Raman scattering, preresonance Raman scattering, resonance Raman scattering, and also infrared and fluorescence.

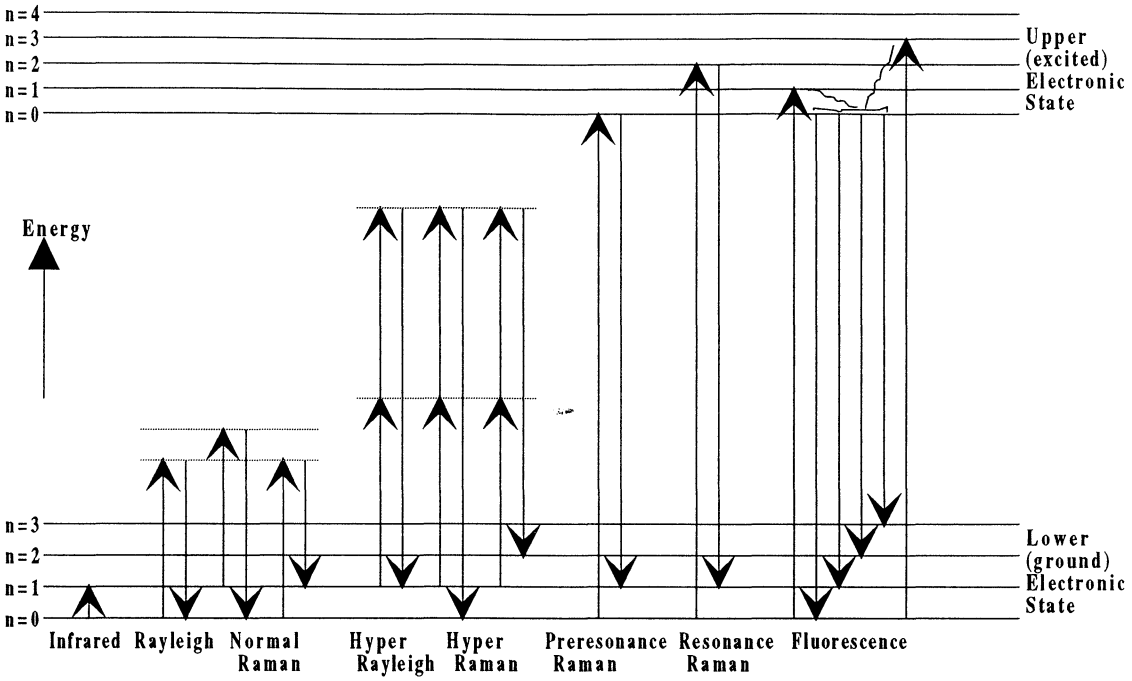

Fig. 2.3 *Some of the possible consequences of light-molecule interaction.*

2.4 Practise of Raman scattering

2.4.1 Introduction

The instrumentation required to undertake Raman spectroscopic studies is actually quite simple. Broken down into its basic components, a Raman experiment consists of a sample, a light source (to irradiate the sample), collection optics (to collect the scattered light), a dispersive optical element (to separate the Raman signals into its constituent wavelengths), and a detection system (to detect the separated Raman signals).

In their first experiments Raman and Krishnan used focused sunlight, coloured glass as filters (to separate a specific wavelength of the sunlight) and visible observation of the colour changes in the scattered light. Soon they changed to, at that time, a more modern arrangement, namely a quartz mercury vapour lamp, a spectrograph, and photographic detection. Using this arrangement Mandelstam and Landsberg reported almost simultaneously as Raman and Krishnan in 1928 that exposure times ranging from 2 to 14 hours was needed to obtain measurable spectra [21]. As a result, the effect was difficult to put to actual use. Despite this, Raman spectroscopy actually flourished, because in these early days the practise of experimental IR spectroscopy was very difficult, while the instrumentation for Raman spectroscopy was readily available as almost the same instrumentation was used as the one in atomic spectroscopy. Then, in the 1950's and 1960's, faster and less expensive IR spectrometers were developed, Raman spectroscopy declined and was practised by only a few specialists.

The situation changed dramatically with the development of the first reliable, commercial continuous wave (CW) visible lasers in the mid-sixties. Now the spectroscopists had access to a monochromatic, coherent, narrow beam and high intensity light source. Together with improvements in spectrometer design and new

detectors this revolutionised Raman spectroscopy. Further developments and improvements, e.g. small and powerful lasers in different wavelength regions, better and sharper filters have made Raman spectroscopy of today an unique and powerful analytical tool, with a wide range of applications [22,23,24,25].

2.4.2 Conventional Raman instrumentation

In order to get a more thorough picture of the instrumentation required to undertake Raman spectroscopic studies we shall start at the light source and work our way along the light path and briefly consider each of the components in turn.

A schematic of the important optics and instrumentation in a conventional Raman scattering experiment is shown in Fig. 2.4.

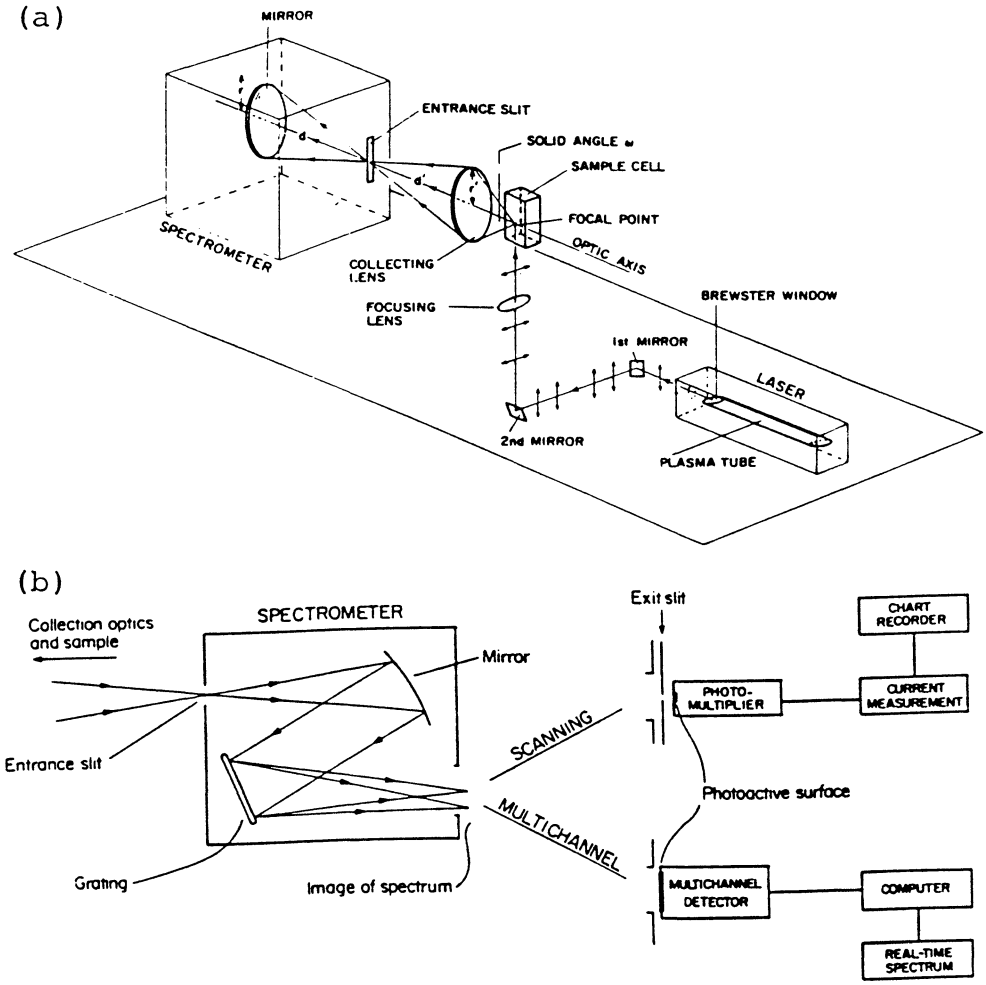

Fig 2.4 *(a) Pre-spectrometer optics and (b) the principle of the spectrometer and detection techniques in a conventional Raman scattering experiment. (From Ref. [25].)*

The light source. Even if it may be possible to obtain satisfactory Raman spectra with light sources other than the laser, it is unquestioned that the laser is the only excitation source that is realistically worth considering. Lasers are conveniently divided into two groups, CW and pulsed laser. CW lasers emit, as the name implies, a continuous stream of light and is by far the most widely used laser for Raman spectroscopy at present time. Pulsed lasers emit a train of short-lived high-power pulses

and is especially used in resonance Raman spectroscopy and time-resolved Raman spectroscopy (cf. time-resolved LIF).

Most applications of Raman scattering of today uses the CW argon or krypton gas ion lasers. These lasers gives a series of lines (excitation wavelengths) in the visible region and offers high output powers. The available lines from the argon and the krypton laser are given in Table 2.1. The obvious reason for using visible excitation in Raman spectroscopy is the ν^4 or λ^{-4} law. Using a laser in the ultraviolet or visible region will give much higher Raman intensity than a laser in the IR region. Another laser is the helium-neon laser operating at 632.8 nm. It has been widely used and is still being used because of its relatively low prize, very robust nature, and air-cooling (an argon and a krypton laser is water cooled). A CW laser can also be used in conjunction with dye lasers. The CW laser then "pumps" the fluorescence spectrum of a dye. Currently available dyes can typically provide Raman excitation from 450 nm to 800 nm.

Table 2.1 *Wavelengths available from Argon and Krypton Ion lasers (nm).*

Argon		**Krypton**	
333.6	465.8	323.9	482.5
334.5	472.7	337.5	520.8
335.9	476.5	350.7	530.9
351.1	488.0	356.4	568.2
351.4	496.5	406.7	647.1
363.8	501.7	413.1	676.5
379.5	514.5	415.4	752.5
454.5	528.7	468.0	793.1
457.9		476.2	799.3

Optics and filters. A CW laser has apart from the individual laser lines also a weak, spurious emission of other outputs, the plasma lines. In order to get rid of these weak lines (which otherwise can produce artefacts in the Raman spectrum) a laser line filter, either a narrow band pass filter or a prism monochromator, is inserted somewhere between the laser and the focusing lens.

A focusing lens is not essential, but as it increases the light intensity at the sample and thus increases the Raman signal it is an obvious advantage to use one. By varying the focal length, one can also change the spot size at the samples. In order to make the collection process simple one usually strives for a small spot size at the sample.

The use of collection optics is of course to collect the scattered light and to direct it onto the spectrometer. The collection optics are usually composed of two lenses (even though in Fig 2.4a only one lens is shown). The light-gathering power of a lens is usually stated in terms of its *f*/-number which is determined by the focal length and the lens diameter (*f*/-number = focal length / lens diameter) and the notation *f*/4.5 means that the focal length of the lens is 4.5 times the diameter. The first lens should have a low *f*/-number so that it collects light from the largest solid angle (as much scattered light as possible). The second lens is used to focus the collected light onto the entrance slit of the spectrometer. This lens should match the *f*/-number of the spectrometer, i.e. it should be placed at a distance d' in front of the slit of the spectrometer so that $d'/r' = d/r$ (see Fig. 2.4a). If this is the case, light from the sample will only just fill the spectrometer optics which is the optimum condition. Overfilling results in loss of Raman signal, and underfilling diminishes the resolving power of the spectrometer. (The resolving power is defined by $R = \lambda/\delta\lambda$, where $\delta\lambda$ is the resulting line width of

the spectral apparatus when using monochromatic light of wavelength λ.)

The spectrometer. The function of the spectrometer is to separate the Raman signals into its constituent wavelengths. The spectrometer in Fig. 2.4b is a basic single spectrometer (one grating) but most Raman experiments use double (two gratings) or even triple (three gratings) spectrometers, because it is essential to effectively separate the Raman signals from the much stronger Rayleigh signal. The double or the triple spectrometer has very high resolution but the major disadvantage of these systems are transmission losses. Even if the Rayleigh signal is effectively separated from the Raman signals, the design also causes loss in the Raman signals.

The optical throughput in a single spectrometer is much higher than in a double or triple spectrometer but so is the stray light from the Rayleigh signal and if a single spectrometer is being used in Raman experiments it is essential that the Rayleigh signal is separated before the scattered light enters the spectrometer. A technique that utilises this approach will be discussed later.

The detection system. As shown in Fig. 2.4b the detection system can be divided into single-channel (scanning) and multi-channel detection. In single-channel detection a scanning spectrometer is used (which by slowly turning the grating scans the lines of the spectrum over the narrow exit slit), a photomultiplier tube (which is an amplifying photocell), a current measuring device (which measures the amplified current from the photomultiplier tube), and some sorts of recording device (which stores the current). The main disadvantage of single-channel detection with a scanning spectrometer and a photomultiplier tube is the time it takes to record a spectrum, but because of the high sensitivity, low background count, reliability, and relatively low cost of the photomultiplier tube, it is still very much in use in many Raman scattering applications.

Multi-channel detection is similar to having several hundred minute photomultiplier tubes across the exit port of the spectrometer. A multichannel detector is, as seen in Fig 2.4b, often connected to a computer because of all the elements - "several hundreds" - that have to be recorded and stored at the same time. The main advantage of multichannel detection is of course that all the spectral elements of interest are observed at the same time. The spectrometer and the multichannel detector arrangement are therefore often referred to as an Optical Multichannel Analyser, OMA. A drawback of a multichannel system is that if one wants high spectral coverage or bandwidth, then resolution must be sacrificed. Another problem is the crosstalk between adjacent elements which also decreases resolution. Examples of multichannel detectors are the photographic plate (hardly used today), the intensified diode array, the charge injection device (CID), and the charge coupled device (CCD).

2.4.3 Fluorescence as a limiting factor in Raman spectroscopy

So far we have not mentioned the major limiting factor in Raman spectroscopy, namely fluorescence. As a phenomenon, fluorescence is approximately 10^6-10^8 times stronger than Raman scattering. As energy splitting between electronic levels in atoms and molecules range from just a few eV up to several keV then it is most likely that fluorescence light will be emitted if a sample is irradiated with visible laser light of 514.5 nm (corresponds to $\approx$ 2.4 eV). The intense fluorescence will then probably totally obscure the much weaker Raman signals.

Extensive efforts have been made to circumvent the problem of fluorescence. One method is sample purification. i.e. to purify the sample as the fluorescence background is often produced by impurities or additives. Another method and probably the oldest one is burning out with the laser beam, which means leaving the sample in the laser beam for several hours. This often results in photobleaching of the sample impurities, but, of course, won't work if the sample itself is fluorescent. One can also use fluorescence quenching agents, i.e. to add a certain compound to suppress, or at least reduce, the fluorescence.

The often very complex molecular structure of tissue makes the influence of fluorescence even more striking, but even so, there are some successful tissue studies using visible excitation and the conventional Raman experimental arrangement discussed in Chap. 2.4.2. Studies of atherosclerotic lesions [26,27] and kidney stones [28,29] with significant fluorescence background have been reported. Also studies of gallstones with no indication of the strength of the fluorescence background [30,31,32] and studies of human breast with weak fluorescence [33] have been performed.

2.4.4 Fluorescence reduction and medical applications

Time-resolved Raman spectroscopy. One fluorescence reduction method is to use the difference in time scales between the process of fluorescence (typically nanoseconds) and Raman (typically picoseconds). Using time-gated techniques it might be possible to discriminate between Raman scattering and fluorescence. This technique is experimentally complex [34] and its applicability to tissue Raman spectroscopy can be questioned, but successful experiments with highly fluorescent compounds have been performed [35].

Wavelength modulation or shifted excitation. Utilising a periodic modulation in wavelength of the excitation irradiation is another effective method to reduce the fluorescence [36]. This method is based on the fact that the narrow Raman band will move with the excitation wavelength, while the fluorescence will remain nearly unchanged. Using a lock-in amplifier a derivative Raman spectrum, almost background free, can be obtained. Instead of a periodic modulation, a simple shifted excitation difference technique can be used [37].

Table 2.2 *Colour, Wavelength, Frequency, Wavenumber, and Energy of Light. (From Ref. [25].)*

Colour	Wavelength (nm)	Frequency (10^{14} Hz)	Wavenumber (cm^{-1})	Energy (kJ/mole)
Near-Infrared	1000	3.00	10 000	120
Red	700	4.28	14 300	171
Orange	620	4.84	16 100	193
Yellow	580	5.17	17 200	206
Green	530	5.66	18 900	226
Blue	470	6.38	21 300	254
Violet	420	7.14	23 800	285
Near Ultraviolet	300	10.0	33 300	399
Far Ultraviolet	200	15.0	50 000	598

UV-excitation. Another fluorescence reduction method is to use UV-excitation (with

increased Raman intensity). The fluorescence background is a broad envelope with a maximum near the centre of the visible region, and with excitation outside this envelope it is sometimes possible to obtain almost fluorescence free spectra. A major problem with UV-excitation is the high energy of the light and as a consequence the high possibility of photodecomposition and the risk of cancerogenous changes of tissue. There are also several fluorophores in the UV-region in tissue. Table 2.2 shows the relationship between wavelength, wavenumber, frequency, energy, and colour of light. UV-excitation below 250 nm of synthetic polymers and without fluorescence background has been reported [38].

Near-infrared excitation. A most useful way to reduce the influence of fluorescence is to use excitation wavelengths in the NIR region (outside the fluorescence envelope). Actually, the optimum wavelength will depend on the sensitivity of the detector, the dark current (noise) of the detector, and the background fluorescence. Recent developments in especially filter design but also in detector and spectrometer design has focused the interest of tissue Raman spectroscopy to the NIR region. Another driving force is the almost negligible risk of photodecomposition and cancerogenous changes of tissue in the NIR region of the electromagnetic spectrum.

Today, excellent Rayleigh line rejection filters in different wavelength regions are readily available, e.g. holographic filters [39,40,41] or semiconductor filters [42,43]. These filters employ a high optical density (O.D. = $\log_{10}(1/\text{transmission})$) at the laser wavelength, over O.D. 4.0, and a narrow transmission slope, over 50 % transmission less than 300 wavenumbers from the laser line. With these filters it has been possible to try new and previously not so efficient experimental methods.

In the IR region almost the only available detectors are single-channel photoconducting detectors which show an increase in electrical conductivity when illuminated with IR light. The wavelength range of these detectors depend on the IR detector material. Examples of IR detector materials and their sensitivity curves are shown in Fig. 2.5. In order to achieve a multiplex measurement (cf. OMA) with single-channel detectors, Fourier Transform (FT) spectroscopy is an obvious choice. FT spectroscopy uses interferometric optics and provides high resolution, wavelength accuracy, and relatively high throughput (a brief description of FT spectroscopy is given in Appendix B).

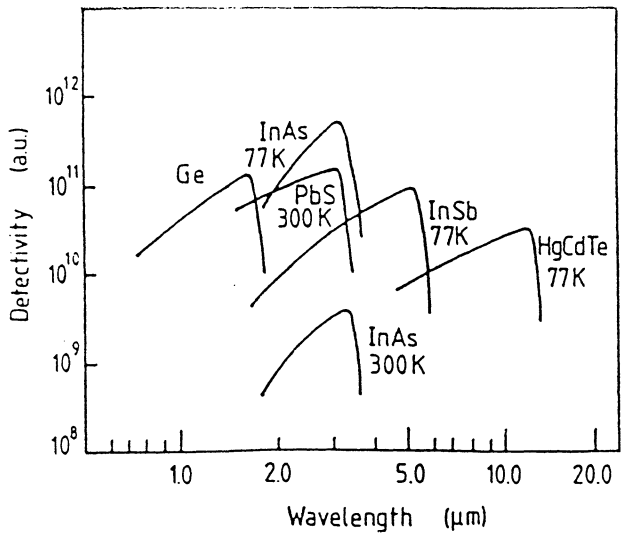

Fig. 2.5 *Sensitivity curves for IR detector materials. (From Ref. [45].)*

An inherent disadvantage of FT spectroscopy is the distributed noise from the Rayleigh scattered light, all the collected light reaches the detector simultaneously, and this has limited the applicability of FT spectroscopy. With the excellent Rayleigh line rejection filters this is no problem whatsoever.

In NIR FT-Raman spectroscopy the sample is exposed to radiation at 1064 nm (Nd:YAG laser) and obtained spectra are virtually free of fluorescence (and Rayleigh distributed noise). The feasibility of the NIR FT-Raman spectroscopy approach was first demonstrated by Hirschfeld and Chase in 1986 [46] and several groups have been active in the field ever since. An instrumental layout for FT-Raman spectroscopy is shown in Fig. 2.6a, while the merit of the method is shown in Fig. 2.6b.

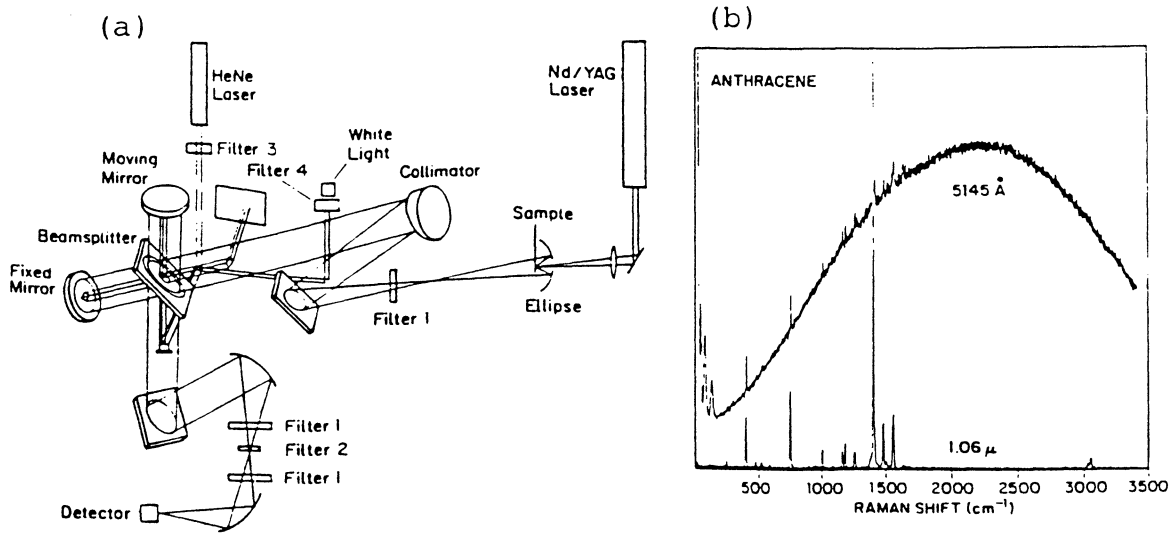

Fig. 2.6 *(a) Instrumental layout for FT-Raman spectroscopy. (b) Top: Raman spectrum of anthracene at 514.5 nm excitation. Bottom: FT-Raman spectrum of anthracene at 1.06 nm excitation (From Ref. [24]).*

NIR FT-Raman spectroscopy have been used for some tissue studies, e.g. gallstone [47], eye lens and different hard tissues [48], normal and cancerous tissue [49], haemoglobin in blood [50], and normal and atherosclerotic tissue [51,52].

NIR FT-Raman spectroscopy has some disadvantages. The relatively high cost for the equipment is one, and that the arrangement consists of moving parts (interferometer) is another. Furthermore the detectors in the NIR region make much more noise than the detectors in the visible region, greatly affecting the signal-to-noise ratio (S/N). A fourth disadvantage is associated with the wavelength and the λ^{-4} dependence. Changing the wavelength from 514.5 nm to 1064 nm decreases the Raman intensity by a factor of 18. For instance, in order to obtain high-quality spectra of normal and atherosclerotic tissue [51,52] it required collection times of 35 minutes and incident powers of 500 mW.

FT spectroscopy at 1064 nm is used to get a multiplex measurement out of a single-channel detector. Instead of making a detour to the FT domains one can use a spectrometer and a multichannel detector directly. It is a fact that no multichannel detectors are sensitive so far into the NIR region as 1064 nm, and in order to use this approach one has to change the excitation wavelength to the 750 - 850 nm region.

A CCD detector is a solid-state multichannel (2-dimensional) sensor that stores photo generated charge carrier packets, exhibits extremely low noise (improves S/N)

and has high quantum efficiency in the 400 nm to 1050 nm spectral region [53]. A typical quantum efficiency curve for a CCD is shown in Fig. 2.7.

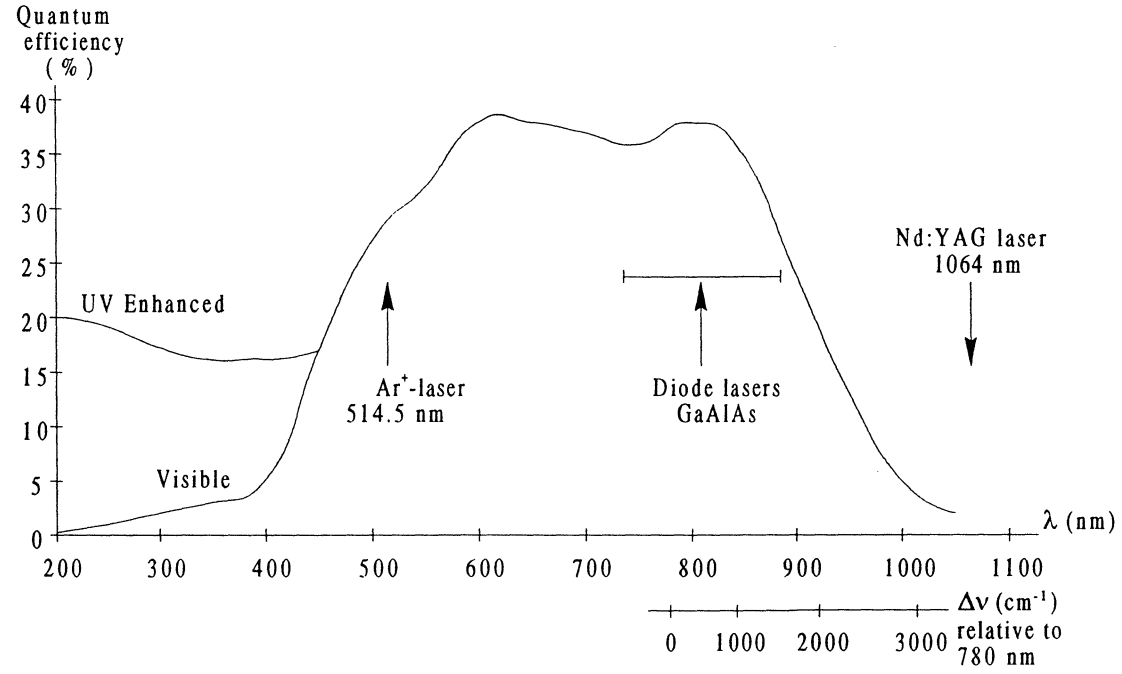

Fig 2.7 *Quantum efficiency curve for a CCD (Thomson CSF THX-31159A). It is possible to extend the sensitivity to the air limit (180 nm) by an UV coating. The Raman shift range for a 780 nm laser is shown. Some laser wavelengths are also indicated.*

A CCD detector, a Rayleigh line rejection filters, and a single spectrometer in the 750 - 850 nm region is an experimental arrangement that takes advantage of the high optical throughput of a single spectrometer with the use of a Rayleigh line rejection filter, uses a detector with high sensitivity and low noise, exhibits less fluorescence compared with that for visible excitation, is relatively cheap, and is compact with no moving parts for a given spectral region.

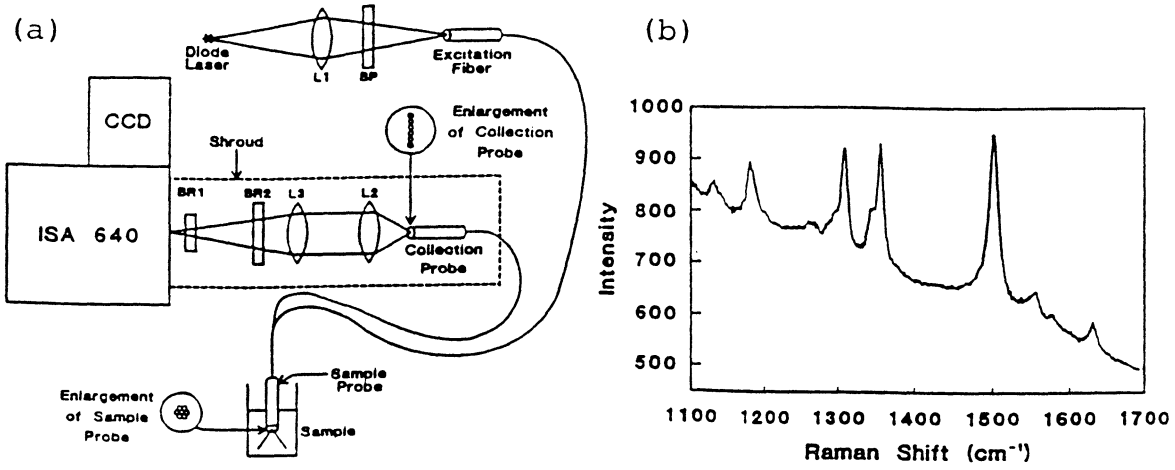

Fig 2.8 *(a) Raman spectroscopy experimental arrangement (L1 , L2, and L3 are lenses and BR and BP are filters). (b) Raman spectrum of Rhodamine 6G (recorded with the experimental arrangement in (a)). (From Ref. [56].)*

The promising aspects of Raman spectroscopy using a CCD detector and diode laser excitation at 780 nm has been demonstrated by McCreery *et al.* [54,55]. Further improvements of the CCD/spectrometer approach, such as fibre optic probes [56,57,58] as well as the robust nature of the equipment greatly increases the versatility and usefulness of this approach. Fig. 2.8a shows a Raman spectroscopy arrangement based on diode laser excitation, fibre optic sampling, spectrometer and CCD detection and Fig 2.8b shows a spectrum of rhodamine 6G, a highly fluorescent laser dye in the region around 500 nm.

NIR excitation using CCD detection have been used in the study of atherosclerotic lesions with a single spectrometer [59] and a double spectrometer [60], and, as expected, there were some fluorescence encountered in the experiments. Fluorescence might still be a major problem in the 750 - 850 nm region compared to 1064 nm excitation and FT-spectroscopy, but the sensitivity (wavelength dependence and the noise) might be much higher. The optimum excitation wavelength depends on, as pointed out before, detector sensitivity, dark current, and background fluorescence and the 750 - 850 nm region is chosen as a compromise between fluorescence reduction and the quantum efficiency of the low noise CCD detector.

2.4.4 Observations of Raman Spectra

An interesting feature of Raman scattering, and a major reason for using Raman spectroscopy in biological studies, is that Raman spectrum of water is weak and rather featureless, and interferes only minimally with Raman spectrum of a solute. This is an obvious advantage in biological and biochemical studies as water always is present to some degree in biological species or biochemical solutions. Also Raman spectrum of glass is weak and featureless, an obvious advantage as well. Raman spectrum of water is shown in Fig. 2.9.

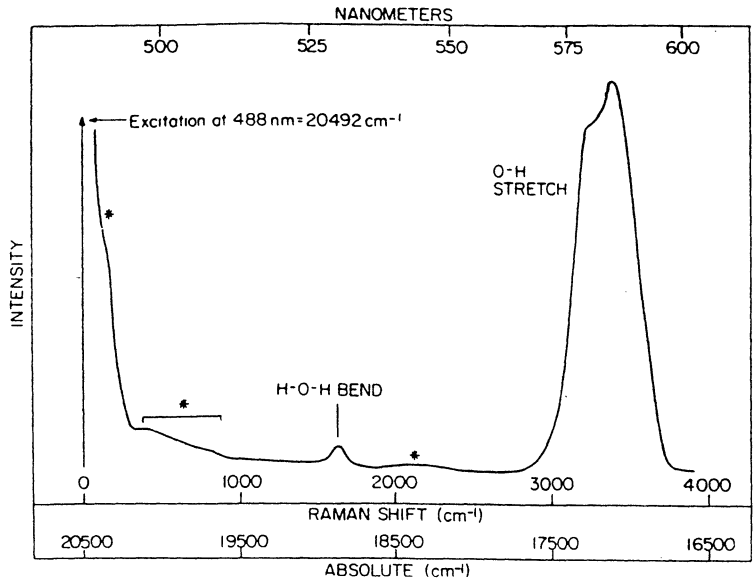

Fig. 2.9 *Raman spectrum of water. The broad features marked with an asterisk are due to interactions between water molecules which are not completely understood. (From Ref. [25].)*

When a Raman spectrum (or an IR spectrum) is to be evaluated it would be of great help if one knew something about the frequency range of and the relative intensities

between different groups of molecules. Using the information about the symmetry of a molecule or a crystal it is possible to predict whether a particular vibrational frequency (also called vibrational mode) is active or not. The symmetry is described in mathematical group theory in terms of point groups. For example, carbontetrachloride CCl_4, which has a tetrahedral structure and which Raman spectrum is shown in Fig. 2.2 belongs to a point group called T_d. A thorough description of group theory and point groups can be found elsewhere, in for instance [13], but one finds that if a molecule has a centre of symmetry, vibrations cannot be active in both IR and Raman. One also finds that, in general, vibrations that do not distort the molecule, symmetric vibrations, are intense in the Raman spectrum (while vibrations that maximise the distortion are most intense in the IR spectrum).

Each atom requires three co-ordinates (the 3 dimensions of space) to describe its position. Every atom has thus three independent degrees of freedom leading to $3N$ degrees of freedom for a molecule containing N atoms. In Raman spectroscopy we are primarily concerned with the vibrational dynamics of a molecule and we can therefore subtract the rotational and translational motions as they do not affect the internal vibrations. Of the $3N$ degrees of freedom of an N-atomic non-linear molecule three describe rotations around the centre of gravity and three describe translations of the centre of gravity. A linear molecule, however, has only two independent rotational degrees of freedom which arises from the fact that rotation about the molecular axis is not considered a degree of freedom since the nuclei is not displaced by such an operation. Thus, a non-linear molecule has $3N$-6 vibrational modes and a linear molecule has $3N$-5 vibrational modes. The vibrational modes in a molecule are conveniently divided into two groups: stretching vibrations, where the distance between the atoms in the molecule is changed, and bending vibrations, where the angle between the atoms in the molecule is changed. Examples of stretching and bending vibrational modes for AX_2 and AX_3 molecular groups are shown in Fig. 2.10.

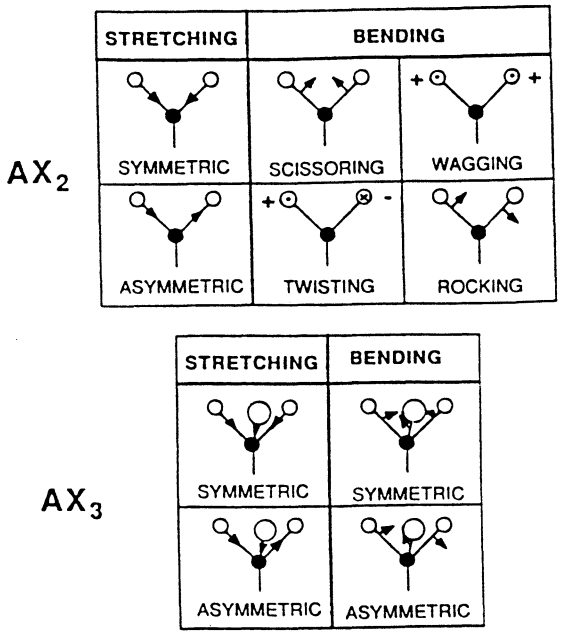

Fig. 2.10 *Stretching and bending vibrational modes for AX_2 and AX_3 molecular groups. (From Ref. [45].)*

The abscissa scale in Raman spectra represents an energy difference between the incoming light and the scattered light. From Fig. 2.9 it is apparent that more energy is

required to bring about the O-H stretching motion than is required for the H-O-H bending motion. It is also apparent from the intensities of the Raman peaks that the O-H stretching mode is more probable to occur than the H-O-H bending mode.

Appendix C. summarises some examples of important vibrational Raman modes and their frequency range (more detailed and exhaustive lists are found in e.g. [13,61,62,63,64]) and on the basis of classical polarisability theory and observations about Raman spectral intensities Nishimura *et al.* [65] have suggested the following rule of thumb:

1. Raman bands are generally more intense for stretching vibrations of covalent bonds than for deformation vibrations.
2. A Raman band assignable to a C=C stretching vibration is stronger than that assignable to a C-C stretching vibration.
3. A Raman band becomes stronger with increase in atomic numbers of the atoms involved in the stretching vibration, all other things being equal.
4. If two bond-stretching motions are involved in a normal co-ordinate, the Raman band is more intense when they take place in-phase than when they take place with 180° phase difference. For a cyclic molecule, the Raman band assignable to a vibration in which all bonds forming the ring stretch and contract in-phase (ring breathing vibration) is usually the strongest one.

2.5 Atherosclerosis

Normal human arteries are composed of three coats. The innermost, or *intima*, consists of a single layer of endothelial cells facing the vessel lumen and a layer of loose connective tissue, mainly made up of collagen fibres. An internal lamina (a thin membrane of elastic fibres) separates the intima from the *media*. The media consists mainly of smooth muscle cells and elastin in various amounts. The amount of elastin increases with vessel size: in the aorta and larger arteries elastin is the major component while in arterioles and small arteries smooth muscle cells are in majority. Another lamina, the external, separates the media from the *adventia*, a thin layer of collective tissue, mainly made up of collagen, lipids and lipoprotein.

The processes involved in atherosclerosis is incompletely understood, but it tends to start with a lesion in the endothelium which permits low density lipoproteins (LDL) containing cholesterol to pass trough [66]. Then the intima thickens, due mainly to accumulation of lipids, smooth muscle cell proliferation and collagen. The lipids deposit deep in the intima while smooth muscle cells and collagen build up a fibrous layer more superficially. As the condition progresses, calcium salts may eventually deposit on the arterial wall and convert the atherosclerotic patches ("plaques") to hard brittle plates. The term atherosclerosis comes from that the lesions consist of a lipid rich part (athere = porridge) and a hard (sclerotic) fibrous part. The structure of an atherosclerotic lesion is shown in Fig. 2.11.

Atherosclerosis occurs in the arteries of all sizes down to approximately 2 mm in diameter. The patches narrow the lumen with consequent chronic ischaemia. Complete occlusion cause infraction, e.g. in the myocardium. Aortic atherosclerosis may ulcerate, and then release lipids or become coated with thrombus, both of which can cause emboli in e.g. kidneys, intestines or legs. Atherosclerosis occurs in some degree in virtually all middle-aged and old people in the developed countries, and accounts for

more deaths than any other disease [66].

Depending on the severity of the atherosclerotic lesion different amounts of deposits are present. Analysing the occurrences of and/or the relationships between e.g. elastin, collagen, lipids, cholesterol, and calcium salts may give an insight in what stage the disease is.

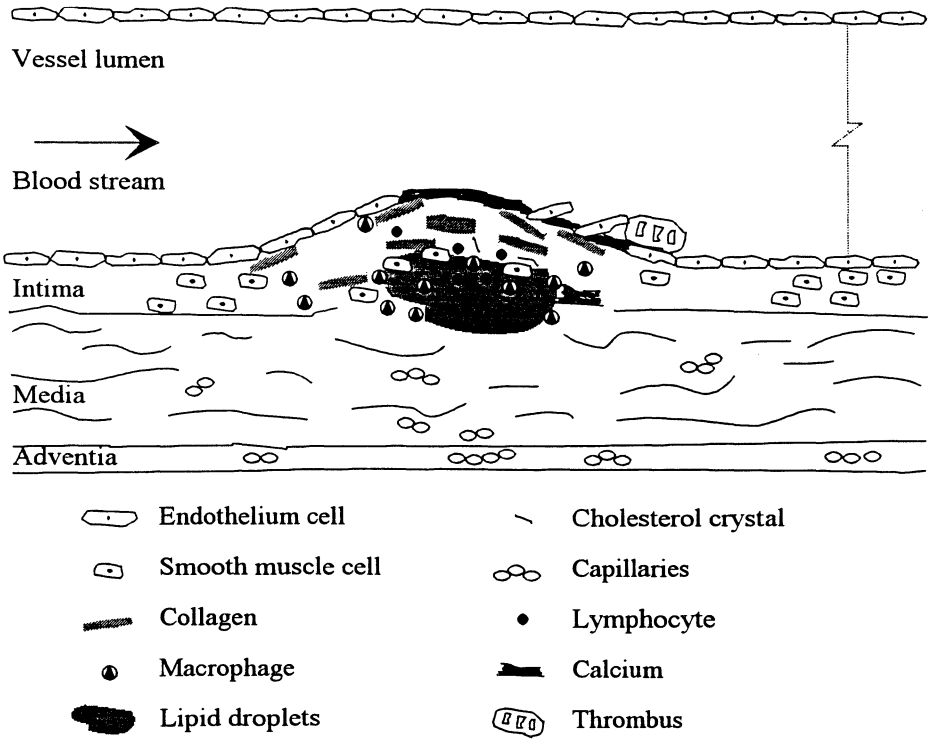

Fig. 2.11 *A diagrammatic cross section through an arterial vessel wall with an atherosclerotic lesion. (From Ref. [67].) Macrophages are large scavenger cells that engulf and digest invading micro-organisms and cell debris, lymphocytes are white blood cells and thrombus is a blood clot.*

2.6 The purpose of this project

The group at the department of atomic physics with research oriented towards laser applications in medicine has not previously performed any research on Raman spectroscopy. As a matter of fact, hardly any Raman spectroscopy research whatsoever has been performed at the department, and the research that has been carried out has used the more conventional experimental arrangement with an argon laser, a monochromater and a photomultiplier.

This project is an initial study of the potential for near-infrared Raman spectroscopy with a charge coupled device detector and a single-stage spectrometer in tissue characterisation and diagnostics, and will hopefully lead to continued research within this area.

The project is focused on the following main subjects;

1. To give an introduction to the theory and practise of Raman scattering and to provide a survey to tissue Raman spectroscopy.

2. To assemble a compact and rugged Raman spectroscopy arrangement based on near-infrared excitation, a single-stage spectrometer and charge coupled device detection with the help of relatively strong Raman scattering samples.

3. To use the Raman spectroscopy arrangement in studies of more complex and highly fluorescent molecules such as laser dyes.

4. Finally, to test the Raman spectroscopy arrangement in tissue characterisation of an atherosclerotic sample from human aorta.

3. Methods and materials

3.1 The experimental arrangements

Two different experimental arrangements have been used. The first, shown in Fig. 3.1, was based on excimer pumped dye-laser excitation and conventional lens optics and the second, shown in Fig. 3.2, was based on diode laser excitation and fibre-optic sampling. Both experimental arrangements used the same single-stage spectrometer and charge coupled device (CCD) detector.

Experimental arrangement no. 1. An excitation wavelength of 730.4 nm was obtained by a dye laser (Lambda Physik FL 2002, Rhodamine 700) pumped by an excimer laser (Lambda Physik EMG 102). The excitation wavelength was chosen as to get the highest possible output power, and the average output power measured at the sample, was 5 mW. The laser beam was focused on the sample with a single lens and the scattered light was collected at 90° to the laser beam axis with a pair of lenses.

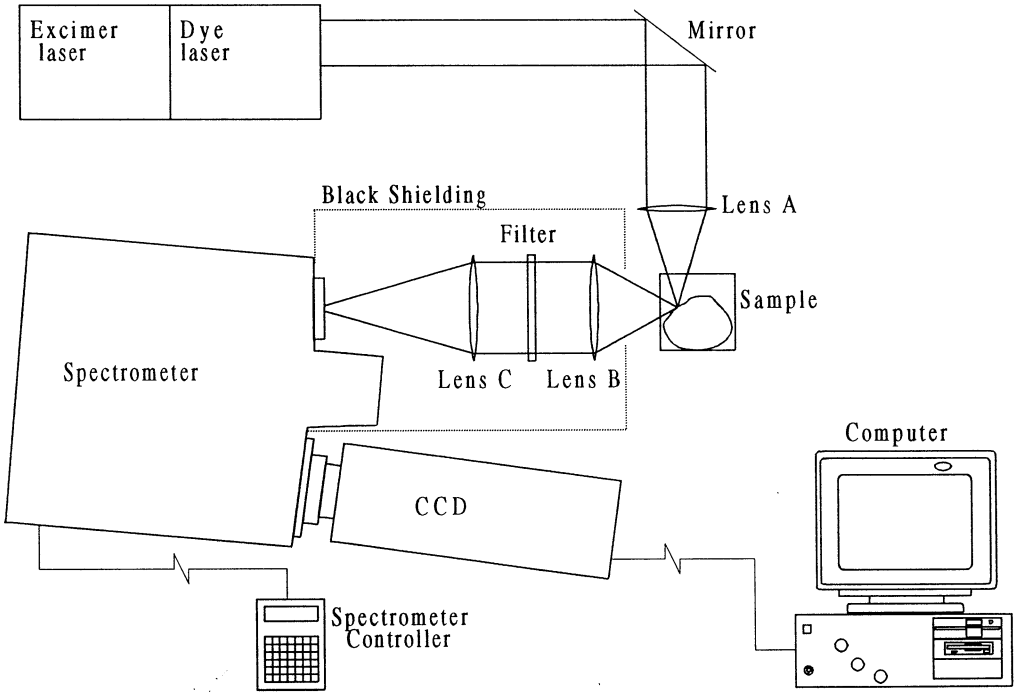

Fig. 3.1 *The experimental arrangement based on dye-laser excitation and conventional lens optics. Lens A, Lens B and, Lens C are Ø 50.8 mm f/2, Ø 100 mm f/1 and Ø 50.8 mm f/1 plano-convex lenses, respectively. Filter is a long pass filter described in the text.*

The elastically scattered light was attenuated prior to the spectrometer with a Schott glass filter (3 mm RG830). The Schott glass filter had an transmission of $2 \cdot 10^{-5}$ at 730.4 nm, 2 % at 800 nm (1200 cm^{-1} from 730.4 nm) and greater than 76 % from 850 nm (1925 cm^{-1}). This wasn't a good filter but among some rather bad filter combinations, this was the one that had the best suppression of the strong Rayleigh line. The collection optics was carefully shielded to reduce unwanted interference

(reflections, background light, etc.).

The alignment of the excitation optics, samples, and collection optics was a complex procedure and had to be reconstructed several times in order to obtain any spectra at all. Another problem was due to the excimer laser. It leaked constantly and had to be refilled more than once a week. (An excimer - excited dimer - laser has a mixture of gases as active medium, and in this case it was XeCl.) Because of the problems and the limited applicability of this experimental arrangement, another arrangement was developed.

Experimental arrangement no. 2. The excitation source was a NIR diode laser (Sharp LTO24MDO). In order to minimise frequency drift the diode laser was operated at 18.6 °C and sometimes at 16.2°C with the use of the Peltier effect. Mode hops of roughly 0.3 nm per °C will otherwise occur [68]. Both the diode laser and the temperature was controlled via an integrated diode laser driver and thermoelectric cooler controller (Melles Griot 06DLD203).

At 18.6°C and 16.2°C the excitation wavelengths were 783.4 nm and 782.0 nm, respectively. The output power, measured at the laser head, was 24 mW, of which approximately 7 mW reached the samples. The principal power losses occurred in the coupling to the excitation fibre and in the band pass filter (Filter 1). The band pass filter was used to remove spurious emission from the diode laser.

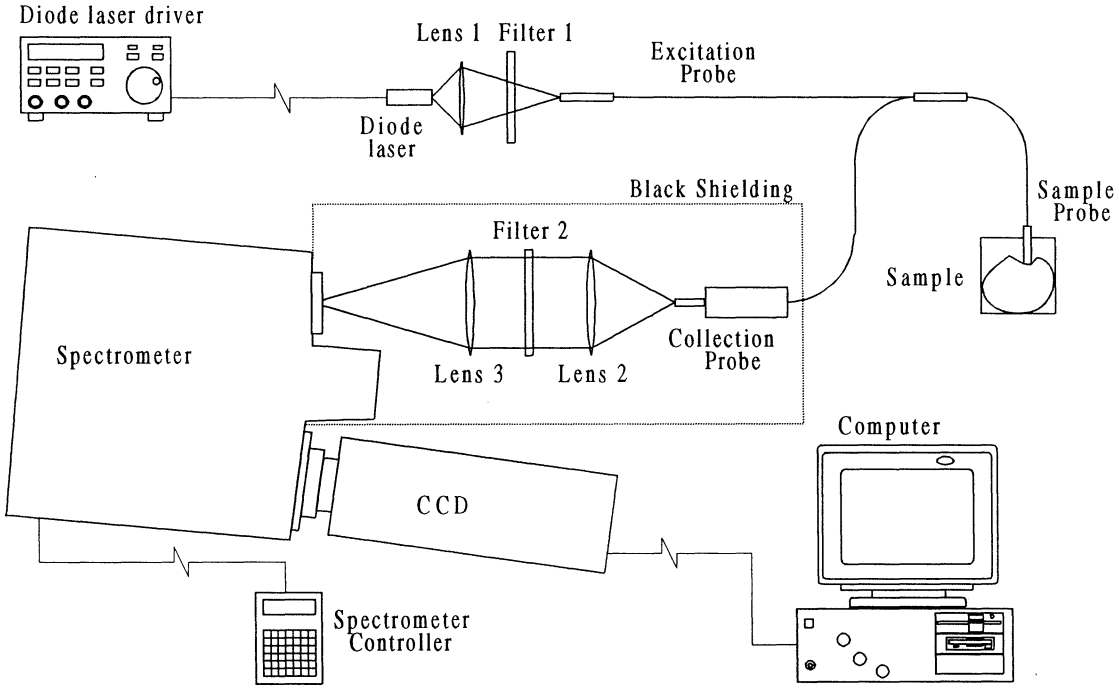

Fig 3.2 *The experimental arrangement based on diode laser excitation and fibre-optic sampling. Lens 1 is a ∅ 8.0 mm collimating and focusing lens, Lens 2 is a ∅ 25.4 f/1 bi-convex lens and, Lens 3 is a ∅ 50.8 f/1 plano-convex lens. Filter 1 is a band pass filter and Filter 2 is a long pass filter.*

The fibre-optic sampler (C-technologies) was originally designed especially for fluorescence spectroscopy but can be used in Raman experiments as well. The excitation probe end consisted of 37 100 μm fibres in a circular array and the sample probe end consisted of the 37 fibres from the excitation probe and 54 100 μm fibres from the collection probe, also in a circular array. In the collection probe end the 54

collection fibres were arranged in a linear array, 6 mm high by 100 μm wide.

The laser beam was focused on the excitation fibres with a collimating and focusing lens (Melles Griot 06GLC002), built onto the diode laser mount. The scattered light was focused onto the spectrometers entrance slit with two lenses. The collection optics was carefully shielded to reduce unwanted interference (reflections, background light, etc.).

The elastically scattered light was attenuated prior to the spectrometer with a Raman holographic edge filter (Physical Optics Corporation). This filter offered a high optical density, OD >5.0, at the laser line and a 80 % transmission +15 nm from the laser line. The filter were designed for a 840 nm laser line, but holographic filters have a tilt and tune capability according to

$$\lambda_s = \lambda\sqrt{1-\frac{\sin^2\theta}{n^2}} \tag{3.1}$$

where λ is the desired wavelength to shift (in this case 840 nm), λ_s is the shifted wavelength (783,4 nm), n is the refraction index (= 1.52), and θ is the required angle to position λ on the edge. Inserting the values, gave that the 840 nm holographic filter should be tilted 33° in order to obtain the same narrow slope for rejection of Rayleigh scattered light at 783,4 nm as for 840 nm.

A problem with the tilt and tune capability of Raman holographic edge filters is that if they shall perform according to specifications, the light must be perfectly collimated. Otherwise the light will pass the filter in different angles, with consequent different degree of attenuation. This was a problem in this experimental arrangement and was almost entirely due to the ∅25.4 mm f/1 bi-convex lens. It might be better to change this lens to another with shorter focal length and greater diameter but in this experimental arrangement the holographic filter was tilted ≈ 25° in order to get as high attenuation as possible of the Rayleigh line and also be able to detect any Raman lines from ≈ 600 cm^{-1} ($\theta \approx 25° \Rightarrow \lambda_s \approx 806$ nm and (1/(783.4nm) - 1/(806+15)nm ≈ 600 cm^{-1}).

Anyhow, this second experimental arrangement was more compact and rugged than the first arrangement. The diode laser was tiny and more user-friendly compared to the big and clumsy excimer/dye lasers, the alignment procedure had to be done only once, and the sample position was not critical.

The spectrometer and the CCD. The scattered light was dispersed by a Spex Model 270M single-stage imaging spectrometer (focal length 0.27m, f/4) and detected and analysed by an EG&G CCD array and optical multichannel analyser (OMA).

The spectrometer utilised two classically ruled gratings, a 150 g/mm grating blazed at 500 nm and a 1200 g/mm grating blazed at 750 nm, with a dispersion of 24.8 nm and 3.1 nm at the focal plane, respectively. The entrance slit of the spectrometer was 1.5 cm high and the width could be set in steps of 6.25 μm between 0 μm 7000 μm.

All moving parts of the spectrometer were automated and controlled remotely by a hand held controller (HandScan).

The CCD array consisted of 512 × 512 elements (pixels) with a total image area of 9.7 mm × 9.7 mm. The 512 vertical pixels were electronically "binned", i.e. they were

summed before readout, resulting in a multichannel detector with 512 channels 9.7 mm high and 19 μm wide. The spectral coverage was thus for the 150 g/mm grating roughly (varies a bit with wavelength) 240 nm or 3000 cm^{-1} from the 783,4-nm laser line and with each pixel covering 5.9 cm^{-1} , and for the 1200 g/mm grating 30 nm or 470 cm^{-1} and 0.9 cm^{-1}/pixel. For the 730.4 nm excitation the spectral coverage was 3400 cm^{-1} and 6.6 cm^{-1}/pixel (150 g/mm) or 540 cm^{-1} and 1.1 cm^{-1}/pixel (1200g/mm).

The CCD was cooled, temperature range from -80 to -140°C, with liquid nitrogen to eliminate dark current. The dark current decreases with temperature, and at -80°C the dark current should be less than 300 photoelectrons per pixel and hour and at -110°C it should be less than 10 photoelectrons per pixel and hour, according to manufacturer specifications. The temperature hold time (= how long time the CCD can be held, locked, at the same temperature) increases with decreasing temperature. Therefore, the temperature should be set as low as possible. Unfortunately the CCD could not hold the temperature according to the specifications, which was 8 hours at -80°C and over 8 hours at -140°C. Actually, the hold time decreased with temperature and was 0 hours at -140°C! If not otherwise stated all Raman spectra were measured with the CCD held at -100°C, with a hold time of approximately 6 hours.

The CCD was controlled by a software acquisition and data handling program (OMA Spec 4000 Applications Software), a controller board (OMA 4 Controller Board), hosted in a personal computer, and a power block (OMA 4 Power Block).

3.2 Data analysis

Experimental arrangement no. 1. The data analysis of the spectra recorded with this experimental arrangement was actually very simple, since neither background subtraction nor any smoothing was applied.

The Raman spectra were typically measured between 400 to 3400 cm^{-1} below the laser frequency with the 150 g/mm grating. No Raman spectra were recorded with the 1200 g/mm grating. The integration time was 300 seconds and the spectrometer slit width was 50 μm.

The wavelength scale was calibrated with the lines from an argon lamp.

Experimental arrangement no. 2. The Raman spectra were measured between 640 and 1840 cm^{-1} below the laser frequency with the 1200 g/mm grating. These spectra are therefore, because of the spectral coverage, composed of 4 successive spectra. No Raman spectra were measured with the 150 g/mm grating.

All spectra were background subtracted but were not corrected for the wavelength-dependent response of the filters, spectrometer and CCD.

The spectrometer entrance slit width was either 50 μm or 100 μm and the CCD integration time was 1 to 300 seconds. The actual slit width and integration time are indicated by each spectrum.

The wavelength scale was calibrated with the lines from an argon lamp.

A shifted excitation difference technique was utilised to improve the fluorescent rejection for some of the highly fluorescent samples. This technique is based on that the narrow Raman band move with the excitation wavelength while the fluorescence remain nearly unchanged. By recording two spectra with slightly different excitation wavelengths and then subtracting these two spectra an almost fluorescent free difference

spectrum can be obtained. The difference spectrum is a derivative spectrum of the Raman spectrum and in order to obtain a conventional Raman spectrum the difference spectrum has to be integrated.

The procedure for the shifted excitation difference technique was: First, a spectrum $S_1(\nu)$ of the Raman scattering and the fluorescence background was recorded with the excitation wavelength, λ_1 = 783.4 nm. Second, another spectrum $S_2(\nu)$ was recorded with the excitation wavelength λ_2 = 782.0 nm by changing the temperature of the diode laser. All other conditions were unchanged. To control any change in laser power and scattering intensity, the two spectra were scaled to the same total area prior to the subtraction. Also prior to the subtraction, the two spectra were smoothed with a median filter 5 pixels wide. Finally the difference spectrum, $D(\nu)=S_1(\nu)-S_2(\nu)$, were integrated to yield a conventional Raman spectrum, $I(\nu)$. Fig. 3.3 shows the principle of the shifted difference technique.

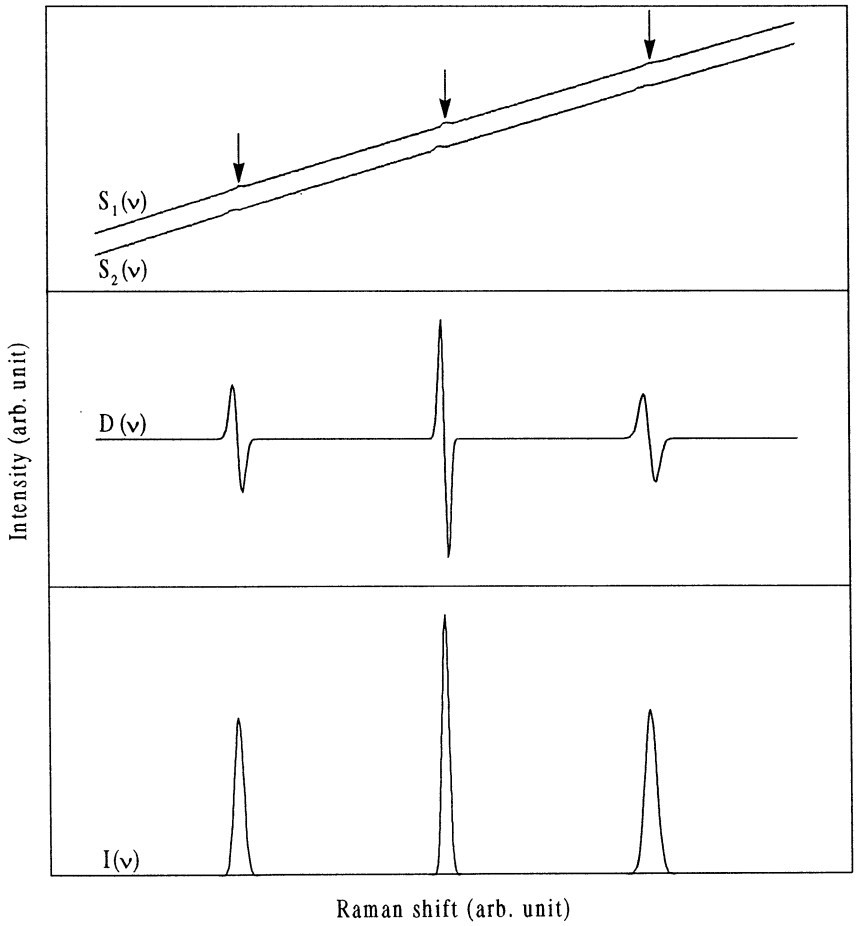

Fig 3.3 *The principle of the shifted excitation difference technique. The arrows indicate three faintly observable Raman peaks.* $S_2(\nu)$ *is offset by a constant for clarity of presentation. The curves presented here are ideal (mathematical functions) and in reality the curves are not this perfect.*

3.3 The samples

Experimental arrangement no. 1. The only samples that were used in this

experimental arrangement were 1,4-dioxane ($C_4H_8O_2$) and toluene (C_7H_8). There was no special reason for the choice of these two solvents, except that they were readily available from the chemical storage room and that their characteristic Raman frequencies are tabulated [38,49]. They are not the strongest Raman scatterers (but not the weakest either) and their structure are relatively simple (but not too simple) which means that the fluorescence interference is minimal. The structure of 1,4-dioxane and toluene are shown in Fig. 3.4.

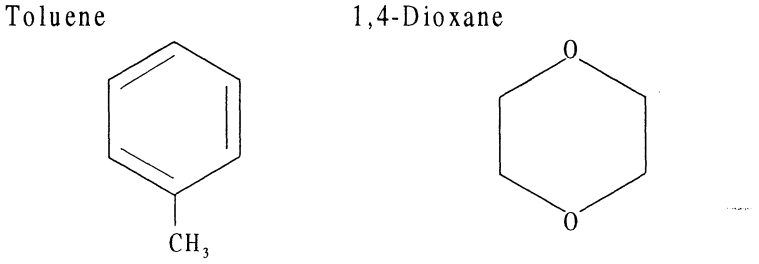

Fig. 3.4 *The structure formula of toluene and 1,4-dioxane.*

Experimental arrangement no. 2. In order to test and optimise the experimental arrangement 1,4-dioxane and toluene were used, for the same reasons as mentioned above.

The laser dyes, rhodamine 6G ($C_{28}H_{31}N_2O_3Cl$) and HITCI ($C_{29}H_{33}N_2I$), were chosen as two examples of more complex and fluorescent samples. If the two samples are used as laser dyes rhodamine 6G is tuneable from 560 to 650 nm while HITCI is tuneable from 810 to 920 nm. The structure of rhodamine 6G and HITCI are shown in Fig. 3.5.

The tissue samples were post-mortem specimens of human aorta supplied by the Department of Pathology, Lund University Hospital. Directly after the excision the "fresh" human aorta samples were brought to the laboratory and rinsed in isotonic saline, and within two to three hours they were examined.

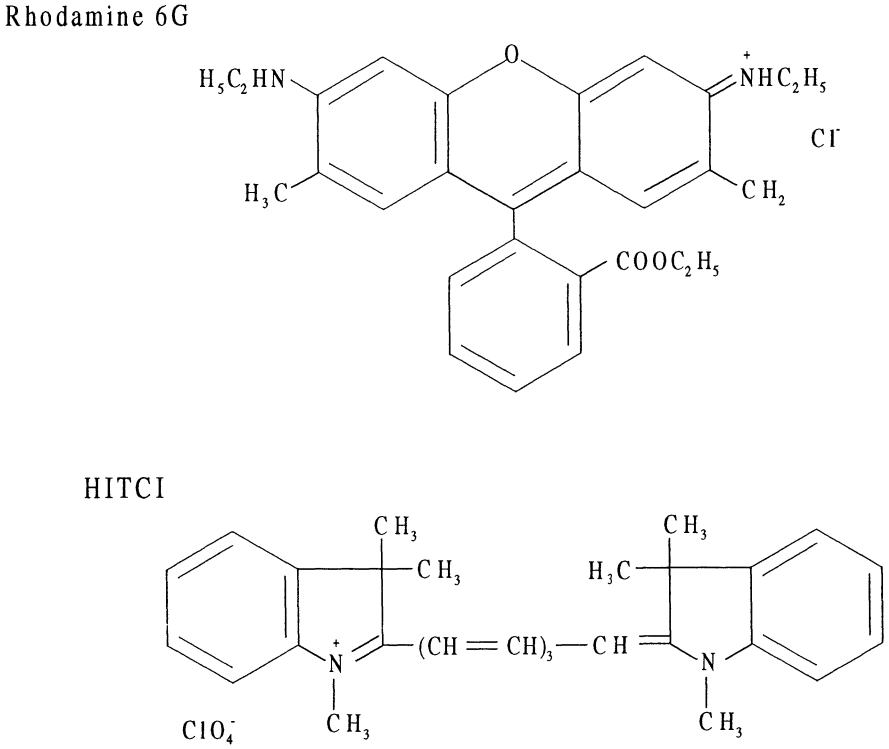

Fig. 3.5 *The structure formula of rhodamine 6G and HITCI.*

4. Results

4.1 1,4-dioxane and toluene

It was, as pointed out before, an elaborate procedure to obtain any Raman spectra at all with 730.4 nm dye laser excitation and conventional lens optics, and actually, the two Raman spectra of 1,4-dioxane and toluene in Fig. 4.1 are the only ones that are really worth presenting.

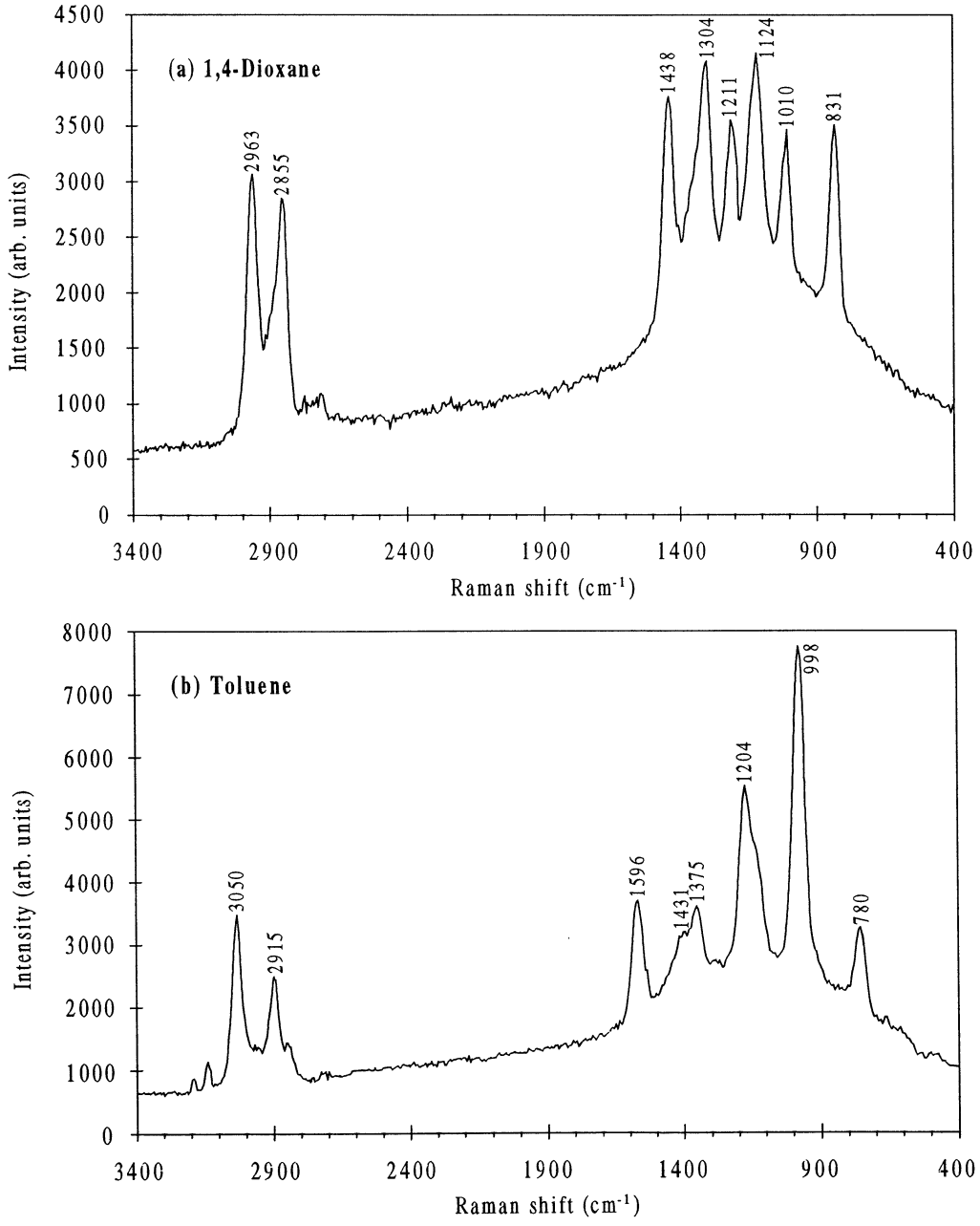

Fig 4.1 *Raman spectra of (a) 1,4-dioxane and (b) toluene with 730.4 nm excitation, 50 μm slit width, 150 g/mm grating, 300 seconds integration time, and -120°C detector temperature.*

More presentable Raman spectra were recorded with 783.4 nm diode laser excitation and fibre optic sampling, and the Raman spectra of 1,4-dioxane and toluene in the region of 640 - 1840 cm^{-1} are shown in Fig. 4.2.

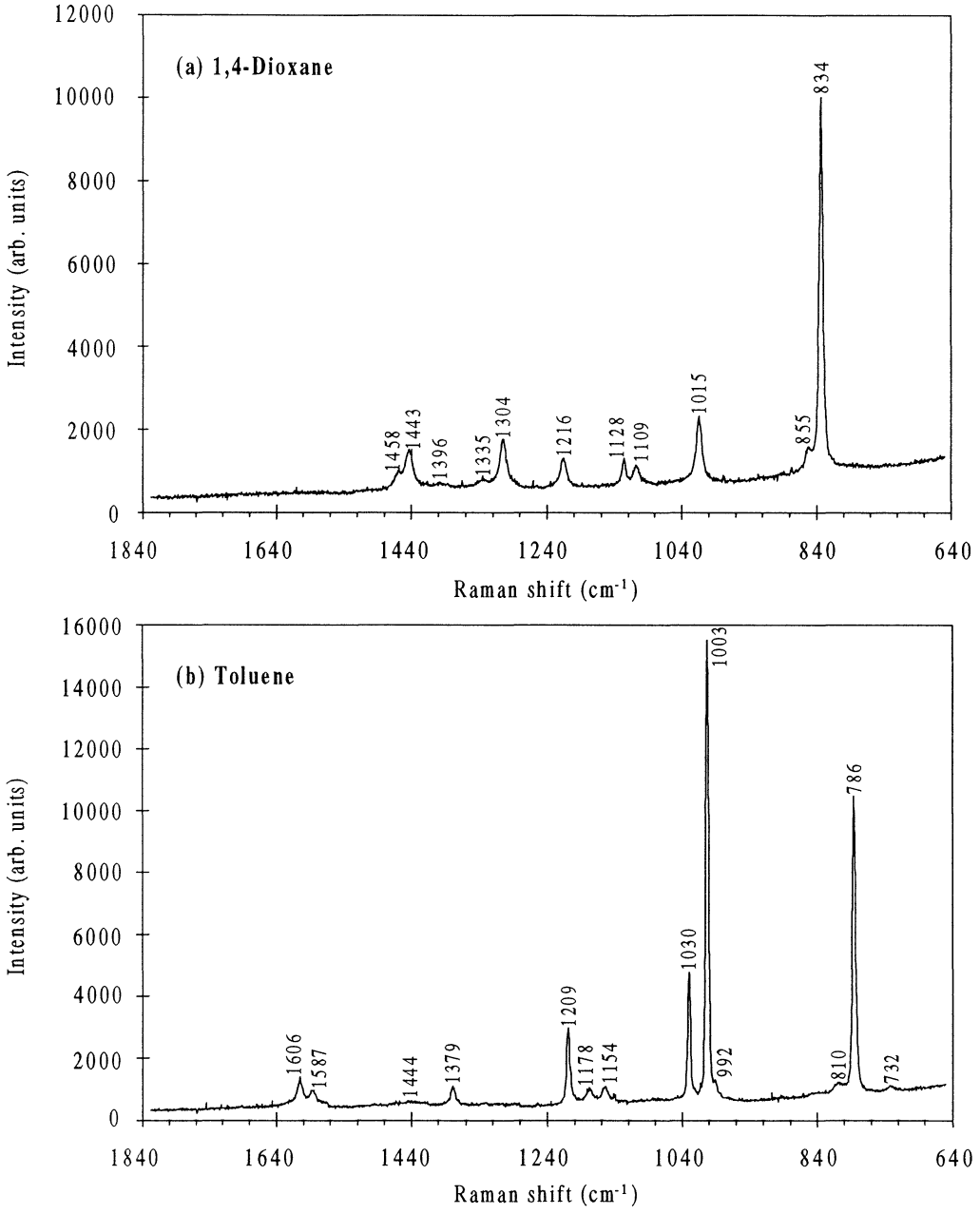

Fig. 4.2 *Raman spectra of (a) 1,4-dioxane and (b) toluene with 783.4 nm excitation, 50 μm slit width, 1200 g/mm grating, and 300 seconds integration time.*

The trade-off between spectral coverage and resolution is obvious from the Raman spectra in Fig. 4.1 and Fig. 4.2. In Fig. 4.1 the entire 400 to 3400 cm^{-1} spectral region is recorded instantly with the 150 g/mm grating, but on the other hand, the resolution is poor. In Fig. 4.2 the resolution is very good with the 1200 g/mm grating, but the spectral coverage is limited, and in order to cover the whole spectral region from 640 to 1840 cm^{-1} four successive spectra has to be recorded.

Fig. 4.3 displays the Raman spectra of 1,4-dioxane and toluene recorded with different integration times. All the major and several minor Raman peaks are still observable with an integration time of 10 seconds.

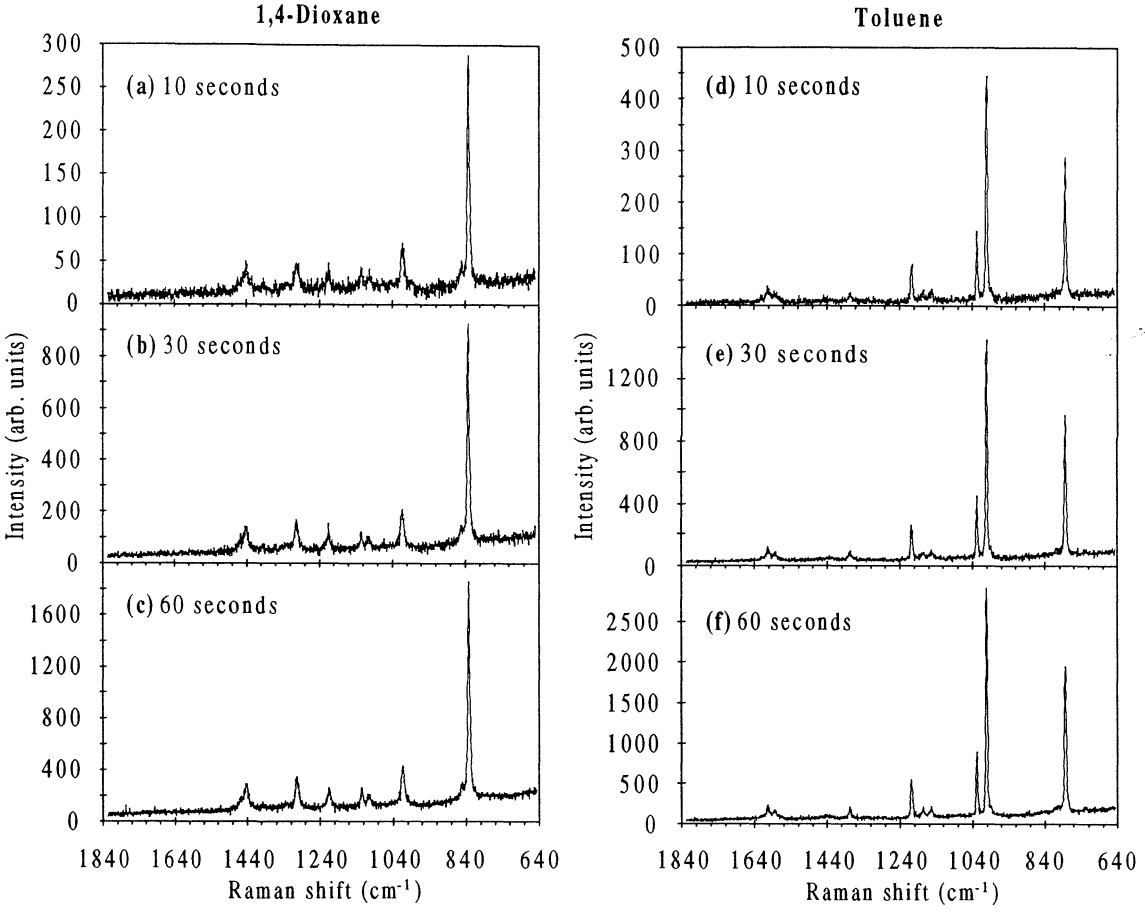

Fig. 4.3 *Raman spectra of 1,4-dioxane and toluene with 783.4 nm excitation, 50 μm slit width, 1200 g/mm grating, and integration times (a, d) 10 seconds, (b, e) 30 seconds, (c, f) 60 seconds.*

The Raman spectra of 1,4-dioxane and toluene in Fig. 4.1 have a similar overall spectral structure with Raman peaks in two relatively distinct spectral regions, 700 to 1700 cm^{-1} and 2800 to 3100 cm^{-1}. The Raman spectra are nevertheless easily distinguishable and show that differences in molecular structure are reflected in the Raman spectra. The different molecular vibrations of 1,4-dioxane and toluene are even more clearly seen in Figs. 4.2 and 4.3.

The Raman peaks, the vibrational bands or modes, are all attributable to a certain molecular vibration, and Table 4.1 lists the band assignment of the observed Raman frequencies of 1,4-dioxane and toluene. References to tabulated Raman frequencies and intensities as well as the observed Raman intensities for 783.4 nm excitation are also given in Table 4.1. It is difficult to say anything for certain about the Raman intensities for 730.4 nm excitation and therefore no conclusion is given. If one recalls the molecular structures of 1,4-dioxane and toluene in Fig. 3.4 and the different vibrational modes in Fig. 2.10 the vibration assignments in Table 4.1 are almost self-explanatory. The ring "breathing" vibration of toluene can be seen as a contradiction of the benzene ring and is typical of benzene and most of the substituted benzenes (among which toluene is one).

Table 4.1 *Observed Raman band frequencies, tabulated Raman band frequencies, Raman band intensities, and band assignment for 1,4-dioxane and toluene.*

1,4-Dioxane

Observed Raman shift[a] (cm^{-1})	Observed Raman shift[b] (cm^{-1})		Tabulated Raman shift[c] (cm^{-1})		Tabulated Raman shift[d] (cm^{-1})		Vibration assignment[d]
831	834	100	833	100	834	vs	Ring stretch
	855	3.5			852	w	CH_2 rock
1010	1015	16	1017	19	1015	s	Ring stretch
	1109	4	1110	6	1109	m	Ring stretch
1124	1128	6	1129	8	1127	m	CH_2 rock
1211	1216	7	1217	9	1216	s	CH_2 twist
1304	1304	12	1302	14	1303	vs	CH_2 twist
	1335	3			1334	m	CH_2 wag
	1396	1			1396	w	CH_2 wag
1438	1443	11	1442	13	1443	vs	CH_2 deformation
	1458	5.5			1461	m	CH_2 deformation
2855			2857	31	2854	vs	Symmetric C-H stretch
2968			2967	31	2966	vs	Anti-symmetric C-H stretch

Toluene

Observed Raman shift[a] (cm^{-1})	Observed Raman shift[b] (cm^{-1})		Tabulated Raman shift[c] (cm^{-1})		Vibration assignment[e]
	732	1			CH deformation o-o-p
780	786	65	788	51	Ring stretch
	810	2			CH deformation o-o-p
	992	1			CH deformation o-o-p
998	1003	100	1001	100	Ring "breathing"
	1030	27	1028	24	CH deformation i-p
	1154	3			CH deformation i-p
	1178	2.5			CH deformation i-p
1204	1209	16	1210	17	C_6H_5-C vibration
1375	1379	4	1380	5	CH_3 symmetric vibration
1431	1444	0.5			CH_3 anti-symmetric vibration
1596	1587	3.5			Ring stretch
	1606	7	1605	6	Ring stretch
2915	2922	10			CH stretch
3050	3054	17			CH stretch

[a] 730.4 nm excitation and 300 seconds integration time.

[b] 783.4 nm excitation and 300 seconds integration time. The band intensities are expressed in percent relative to the strongest band.

[c] From Ref. [64]. The band intensities are expressed in percent relative to the strongest band.

[d] From Ref. [63]. Abbreviations: vs=very strong, s=strong, m=medium, and w=weak relative band intensity

[e] From Ref. [13,61,62,63]. Abbreviations: o-o-p=out-of-plane and i-p=in-plane.

4.2 Laser dyes

Fig 4.4 displays the NIR Raman spectrum of rhodamine 6G. The background is higher than in the Raman spectra of 1,4-dioxane, but the Raman peaks are still easily discernible from the background. More vibrational bands are of course also observable for the relatively complex molecule rhodamine 6G than for the simpler molecules 1,4-dioxane and toluene.

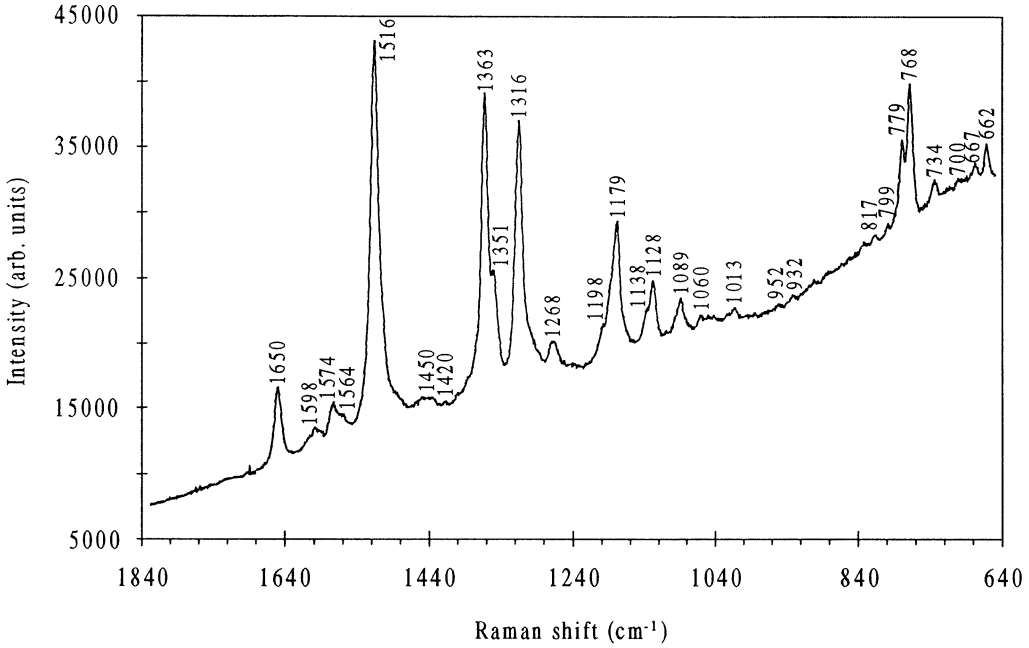

Fig. 4.4 *Raman spectrum of rhodamine 6G with 783.4 nm excitation, 50 μm slit width, 1200 g/mm grating, and 60 seconds integration time.*

The 65-atomic molecule rhodamine 6G has a total of 189 vibrational modes while 1,4-dioxane and toluene have 36 and 39 vibrational modes, respectively. All of these vibrations are not Raman active, but it gives an idea of the complexity and the difficulties connected with vibration assignment of the Raman spectrum of rhodamine 6G, and actually, no band assignment has been carried out. How many vibrations that actually are Raman active for rhodamine 6G has not been possible to deduce, but at least 28 active vibrational Raman modes in the limited spectral region 640 - 1840 cm^{-1} are shown in Fig. 4.4. The Raman band frequencies and intensities of the 28 observed vibrational modes are listed in Table 4.2.

Table 4.2 *Observed Raman band frequencies and intensities of rhodamine 6g.*

Raman shift (cm^{-1})	Relative Intensity (%)	Raman shift (cm^{-1})	Relative Intensity (%)	Raman shift (cm^{-1})	Relative Intensity (%)	Raman shift (cm^{-1})	Relative Intensity (%)
662	7	817	2	1138	9	1420	1
677	3	932	2	1179	35	1450	4
700	1.5	952	1	1198	9	1516	100
734	5	1013	3	1268	8	1564	6
768	35	1060	2	1316	68	1574	10
779	22	1089	10	1351	25	1598	6
799	2	1128	16	1363	77	1650	19

Fig. 4.5 shows Raman spectra of rhodamine 6G with different integration times and as for 1,4-dioxane and toluene all the major and several minor Raman bands are observable with an integration of 10 seconds. With 1 second integration time only the major Raman peaks are discernible from the background.

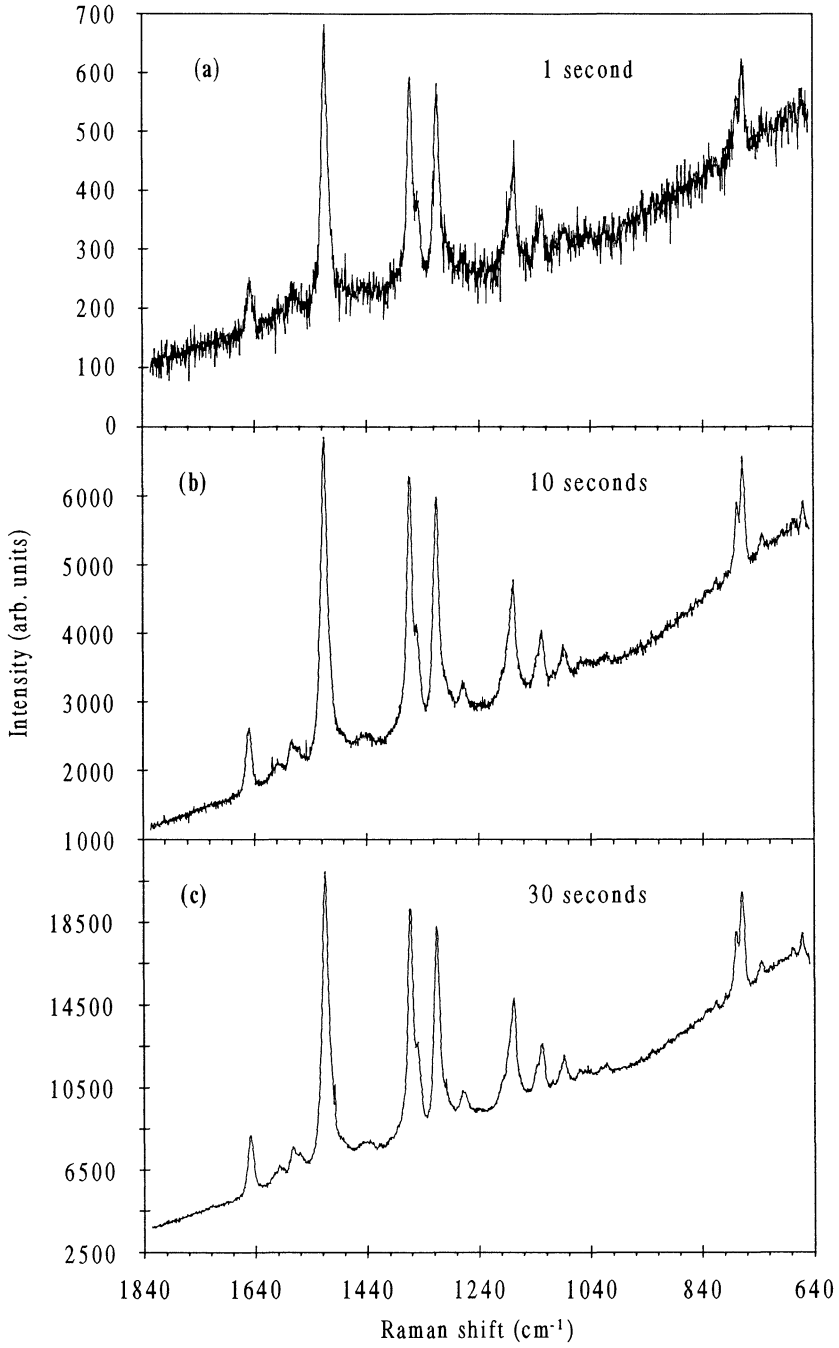

Fig. 4.5 *Raman spectra of rhodamine 6G with 783.4 nm excitation, 50 μm slit width, 1200 g/mm grating, and (a) 1 second, (b) 10 seconds, and (c) 30 seconds integration time.*

It was expected that the fluorescence background of HITCI should be considerably higher than that of 1,4-dioxane, toluene and rhodamine 6G, and this was also the case. The Raman peaks can faintly be discernible from the broad-band fluorescence background and in order to reduce this background and to resolve the Raman peaks better the shifted excitation difference technique was implemented.

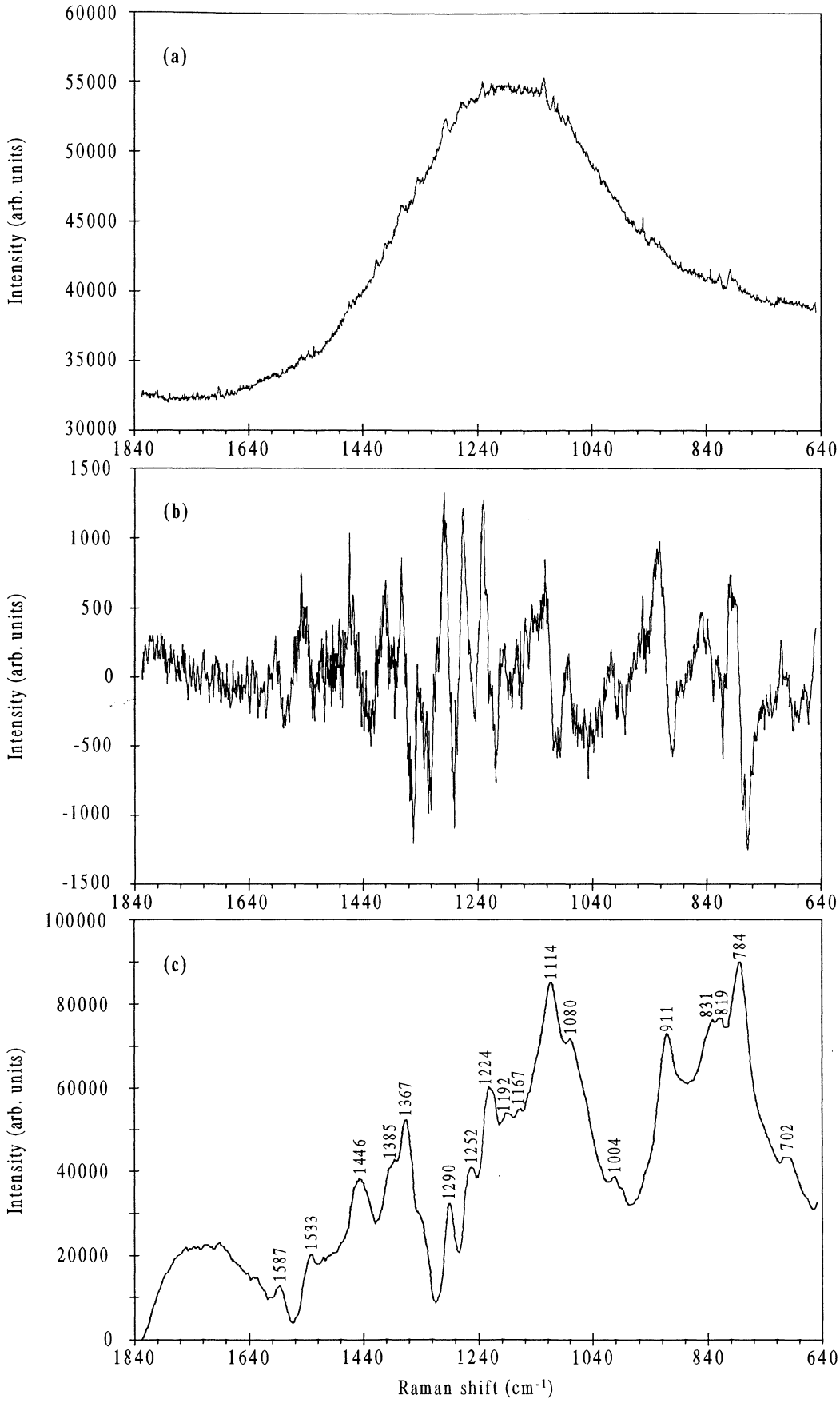

Fig. 4.6 *(a) Emission spectrum of HITCI with 783.4 nm excitation, 100 μm slit width, 1200 g/mm grating, and 300 seconds integration time. (b) Difference spectrum of emission spectra of HITCI excited with 783.4 nm and 782.0 nm. (c) Integrated difference spectrum.*

Fig. 4.6 displays the 783.4 nm excited Raman spectra, the difference Raman spectra, and the integrated Raman spectra of HITCI. It is apparent from Figs. 4.6a and 4.6c that the identification of the Raman band frequencies is more easily performed in Fig. 4.6c. One can also see that the integration procedure in the shifted excitation difference technique smoothes the Raman spectra and causes some line width broadening.

No band assignment or relative intensity calculations of the Raman frequencies of HITCI has been performed. Nor has any Raman spectra with different integration times been recorded.

4.3 Human aorta

Now we are supposed to have come to the most interesting part of this project, but unfortunately the results are not very good. Not very good is an idealisation of the actual situation, as none of the recorded Raman spectra of human aorta are presentable. Something happened with the experimental arrangement between the testings of HITCI and the samples from human aorta. No matter what sample or region of the sample (healthy, mildly atherosclerotic, severely atherosclerotic or lipid rich tissue), the Raman were almost identical. The Raman spectra have no structure at all and not even the shifted excitation difference technique reveal any hidden Raman bands.

Despite extensive efforts (for further information see Chap. 5.2) no solution of the problem with structureless Raman spectra are in sight, and as time is running away with this project, I have decided to put an end to the project here. I am however convinced that the quality of the spectra from the tissue samples can be substantially improved and that the poor quality is due to problems with the equipment rather than with the samples.

5 Discussion and conclusions

5.1 The results

The results presented here clearly show that NIR infrared Raman spectroscopy with a single spectrometer and CCD detector is a very sensitive arrangement and accordingly has an enormous potential as a monitor of molecular chemistry.

It is interesting to note that, even with excitation wavelengths in the NIR region and with moderate (diode) laser powers, most of the weaker as well as all the strong, Raman bands in 1,4-dioxane and toluene can be observed with an integration time of 10 seconds. The major vibrational bands in rhodamine 6G can be observed with an integration time as short as 1 second, but in order to observe the finer aspects of rhodamine 6G an integration time of at least 10 seconds is required.

It is also interesting to note that the fluorescence interference in the Raman spectra of rhodamine is no problem at all. Even if fluorescence is encountered, it does not obscure the Raman bands.

In the Raman spectra of the more fluorescent laser dye HITCI, the fluorescence interference is still a major obstacle. It is impossible to say wether tissue fluorescence is as strong as HITCI fluorescence without any Raman spectra of tissue for comparison. The shifted excitation difference technique is one way to conveniently overcome the fluorescent intereference, but in order to obtain high quality integrated Raman spectra an integration time of 300 seconds is required.

A stronger laser will undoubtedly decrease the integration time, and perhaps a slight increase in excitation wavelength will reduce the fluorescence interference and also the collection time. A wavelength change to around 800 nm is optimal, as a further increase will considerably decrease the efficiency of the CCD detector. These considerations call for further experiments and investigations.

The trade-off between spectral coverage and resolution also determines the *total* integration time. The one second Raman spectrum of rhodamine 6G has an total integration time of 4 seconds as the spectrum is composed of four successive spectra with an integration time of 1 second each. It is apparent that resolution has to be sacrificed if a high spectral coverage and a short total integration time is desirable. It is also apparent that if high resolution *and* a short total integration time are required, then the spectral coverage has to be sacrificed.

5.2 Problems

It is no understatement to say that a significant part of this project has concerned itself with problems. The constant leakage from the excimer laser was one problem, the material procurements and delivery times, another. Maybe this is not considered a problem, but if one has to wait 1-2 months (for items that are essential for the experiments) when a delivery time of only 1-2 weeks has been promised, then it certainly becomes a problem. Without the ordered items (e.g. the Raman holographic

edge filter and the Peltier element for the diode laser) it was impossible to conduct any experiments and the whole project was put on hold until they arrived. These impediments are settled now, the excimer/dye laser system has been replaced by the diode laser, and the Raman filter and the Peltier element has arrived, but there are still obstacles that remain unsolved.

One unsettled problem is caused by the CCD detector which cannot hold the temperature given by the manufacturer specifications. The CCD detector is, as mentioned before, controlled by a software acquisition and data handling program (OMA Spec 4000 Applications Software). The temperature levels for the CCD detector are set in increments of 2°C between -80°C and -140°C. Lower temperatures reduce dark current and therefore is it desirable to set the detector temperature as low as possible. Until the set temperature is reached a status bar on the computer screen reads *Unlocked.* When the set temperature is reached the status bar changes to *Locked*, so one can always see if the detector temperature is stabile or not.

When the CCD detector was delivered the hold time was 2-3 hours at -120°C and 7-8 hours at -80°C. This problem was temporarily solved with a factory repair - the vacuum around the liquid nitrogen container, the dewar, was restored. Directly after the repair the CCD detector hold time was 6-7 hours at -120°C, but that only three months after the repair the hold time at -120°C was even shorter than before, namely less than one hour. By changing the temperature to -100°C a hold time of 6-7 hours was achieved. The performance of the CCD detector has not been further degraded and is today, eight months after the repair, the same as after three months. The CCD detector has never locked at -140°C, neither before nor after the repair.

The CCD hold time at -100°C can be extended by regularly refilling the dewar - every fourth hour is advisable. The hold time at -120°C cannot be extended by such a refill. The Unlocked indication always appears within one hour after the Locked indication. The only way to receive the Locked indication once again at -120°C is to turn off the software program for half an hour and then turn it on again. As this manoeuvre has to be performed every hour, it is no alternative to a regular refilling (without software restart) at -100°C.

Another factory repair might have solved this problem, but as a factory repair takes at least one month, a decision was made not to waste valuable experiment time but to postpone the repair until this project was completed.

Another drawback and without question the most severe one is the problem with the structureless Raman spectra discussed in Chap. 4.3. After the successfully recorded Raman spectra of HITCI something happened with the expereimental arrangement.

Fig. 5.1 shows an "emission" spectrum of an aluminium foil with 789 nm diode laser excitation and the 150 g/mm grating. Approximately 40 nm next to the laser line there is a broadband "emission". This broadband "emission" also is encountered in the Raman spectra from human aorta and totally obscures the Raman bands. It is not clear what the phenomenon is and without no better name, it will be called "emission" or background "emission". The "emission" is wavelength dependent, i.e. the same spectral structure is seen with the 1200 g/mm grating (not shown here).

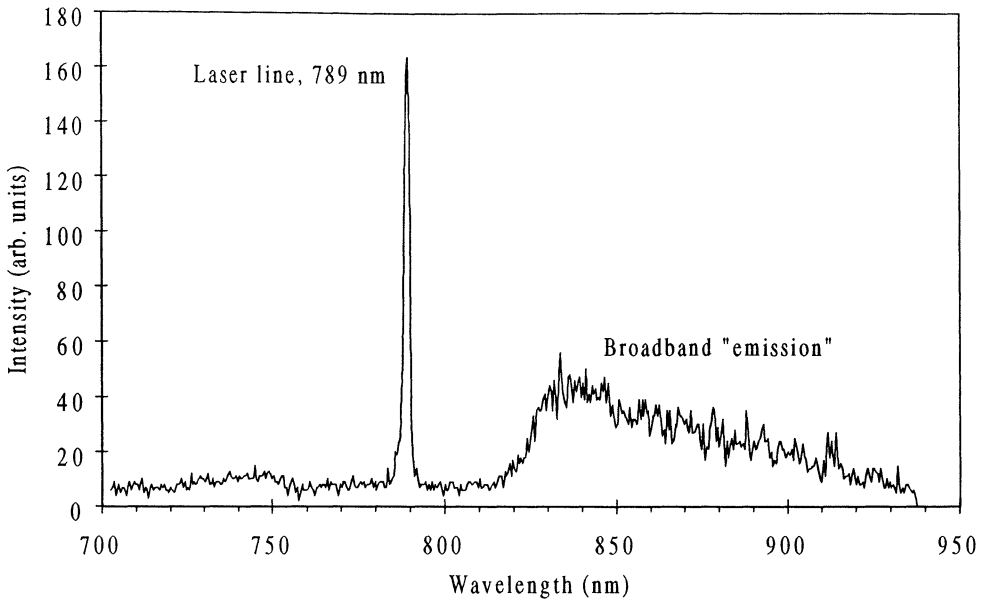

Fig. 5.1 *"Emission" spectra of an aluminium foil. Recorded with exactly the same experimental arrangement (no. 2) as for the Raman spectra of 1,4-dioxane, toluene, rhodamine 6g, and HITCI in Chap. 4 except that another Sharp diode laser has been used.*

A broadband "emission" that totally obscures the Raman bands has been encountered from the beginning of this project. Only twice has it been possible to obtain any Raman spectra at all; once when the Raman spectra of 1,4-dioxane and toluene with 730.4 nm excitation was recorded, and then when the Raman spectra of 1,4-dioxane, toluene, rhodamine 6G and HITCI were recorded. Otherwise this broadband "emission" was the only structure that could be seen.

At first, rediffracted light from the laser line in the spectrometer was considered to be the probable cause of the broadband "emission", but this light can be removed with proper filtering of the laser line. Today the light is no problem, but even so a broadband "emission" is encountered. For further observations about rediffracted light in the spectrometer, see Appendix D.

The following changes and tests, and combinations of them, in the experimental arrangement (no. 2) have been tried several times, but without any success:

1. Realigning the collection and excitation optics.
2. Changing the diode laser. Two Sharp diode lasers (at 783 nm and 789 nm) and two Mitsubishi diode laser (both at 789 nm) has been tried.
3. Changing the band pass filter after the diode laser.
4. Trying with two band pass filters after the diode laser.
5. Removing the band pass filter.
6. Inserting a small tube of black paper between the diode laser and the excitation probe in order to remove the possibility of rediffracted light outside the spectrometer.
7. Using two Schott filters (RG780 5 mm and RG830 3 mm) instead of the Raman holographic filter.
8. Changing the two lenses in the collection optics to a 50 mm f/1.8 camera lens and 50.8 mm f/2 planoconvex lens.
9. Removing the fibre optic sampler and using conventional lens optics.

10. Trying with a HeNe-laser with two Schott filters (RG630 3 mm and RG695 3 mm) before the spectrometer instead of the diode lasers.
11. Cleaning the entrance slit of the spectrometer.

It is extremely frustrating not being able to solve the problem with the background "emission". I have run out of ideas of solution, but I strongly suspect that the problem is in some way connected with the equipment and then especially with the spectrometer. But if it is the spectrometer, another, even greater question arises: *How have I then been able to obtain any Raman spectra at all?*

It is a fact that Raman spectra of 1,4-dioxane, toulene, rhodamine 6G, and HITCI have been recorded, but I have not the faintest idea why it would only function sometimes and not always. Whatever the right answer of the background "emission" really is, there is at least one thing I do know: I have not found it.

5.3 The future

With a major problem still unsolved it is hard to say anything certain about the future. Probably the best action to take is to change the spectrometer. Hopefully this will overcome the problem and lead to fine Raman spectra of tissue.

Other possible actions to take is to use more powerful diode lasers, to optimise the excitation and collection optics and fibre samplers, and to use a 450 g/mm grating for instance instead of a 1200 g/mm (greater spectral coverage) or a 150 g/mm grating (better resolution), so that it might be possible to obtain Raman spectra of both fluorescent and non-fluorescent samples with integration times that are less than one seconds.

5.4 Conclusions

With low powered NIR dye laser excitation, conventional lens optics, a single spectrometer, and a CCD detector, collection times of 300 seconds are required to obtain high quality Raman spectra of 1,4-dioxan and toluene.

By using low powered NIR diode laser excitation, a fibre optic sampler, a single spectrometer and a CCD detector it is possible to obtain high quality Raman spectra of 1,4-dioxane, toulene, and rhodamine 6G with a collection time of 10 seconds or less.

With a shifted excitation difference technique the fluorescence interference can be significantly reduced in Raman spectra of highly fluorescent laser dye such as HITCI.

6 Acknowledgements

First, I would like to thank my supervisor Stefan Andersson-Engels who has guided me through this project.

I would also like to thank Jonas Johansson, who kept me company during many hard weekends, and who gave me good advice and help on various occasions.

I am grateful to Roger Berg who has shared his computer skills with me, and to Peter Kauranen, who was very helpful when it came to questions about diode lasers and their characteristics.

During the many hours I have spent in the laboratory struggling with various problems, it has been very good to have Claes af Klinteberg and Annika Nilsson to talk to.

I would like to thank Sune Svanberg, who initiated my interest in this field of physics and who is a constant source of encouragement.

Finally, I would like to thank those not mentioned by name, but who in one way or another have helped and encouraged me during this project.

7. List of references

1. S. Andersson-Engels, R. Berg, J. Johansson, U. Stenram, K. Svanberg, and S. Svanberg, *Laser Spectroscopy in Medical Diagnostics*, in B.W. Henderson and T.J. Dougherty (eds.), *Photodynamic Therapy*, Marcel Dekker, New York, 387-424 (1992).

2. S. Andersson-Engels and B.C. Wilson, *In vivo Fluorescence in Clinical Oncology: Fundamentals and Practical Issues*, Journal of Cell Pharmacology **3**, 48-61 (1992).

3. L.I. Deckelbaum, M.L. Stetz, K.M. O'Brien, F.W. Cutrozzola, A.F. Gmitro, L.I. Laifer, and G.R. Gindi, *Fluorescence Spectroscopy Guidance of Laser Ablation of Atherosclerotic Plaque*, Lasers in Surgery and Medicine **9**, 205-214 (1989).

4. M. Scheu, H. Kagel, M. Zwaan, A. Lebeau, and R. Engelhardt, *A New Concept for a Realtime Feedback System in Angioplasty With a Flashlamp Pumped Dye Laser*, Lasers in Surgery and Medicine **11**, 133-140 (1991).

5. P. Teng, N.S. Nishioka, R.R. Anderson, and T.F. Deutsch, *Optical Studies of Pulsed Laser Fragmention of Urinary and Biliary Calculi*, Lasers in Life Sciences **1**, 231-245 (1987).

6. C. Palmqvist, *Laser Lithiotropsy of Kidney Calculi with Nd:YAG Laser*, Diploma Paper, Lund Reports on Atomic Physics **LRAP-94** (1988).

7. R.R. Alfano, W. Lam, H.J. Zarrabi, M.A. Alfano, J. Cordero, D.B. Tata, and C.E. Swenberg, *Human Teeth with and without Caries Studied by Laser Scattering, Fluorescence, and Absorption Spectroscopy*, IEEE Journal of Quantum Electronics **20**, 1512-1516 (1984).

8. F. Sundström, K. Fredriksson, S. Montán, U. Hafström-Björkman, and J. Ström, *Laser-Induced Fluorescence from Sound and Caries Tooth Substances: Spectroscopic Studies*, Swedish Dental Journal **9**, 71-80 (1985).

9. S. Andersson-Engels, J. Johansson, U. Stenram, K. Svanberg, and S. Svanberg, *Time-Resolved Laser-Induced Fluorescence Spectroscopy for Enhanced Demarcation of Human Atherosclerotic Plaque*, Journal of Photochemistry and Photobiology B: Biology **4**, 363-369 (1990).

10. S. Andersson-Engels, J. Johansson, and S. Svanberg, *The Use of Time-Resolved Fluorescence for Diagnosis of Atherosclerotic Plaque and Malignant Tumours*, Spectrochimica Acta **46A**, 1203-1210 (1990).

11. S. Andersson-Engels, R. Berg, and S. Svanberg, *Effects of Optical Constants on Time-Gated Transillumination of Tissue and Tissue-Like Media*, Journal of Photochemistry and Photobiology B: Biology **16**, 155-167 (1992).

12. R. Berg, O. Jarlman, and S. Svanberg, *Medical Transillumination Imaging Using Short-Pulse Diode Lasers*, Applied Optics **32**, 574-579 (1993).

13. N.B.Colthup, L.H. Daily, and S.E. Wiberly, *Introduction to Infrared and Raman Spectroscopy*, Academic Press, San Diego (1990).

14. B.R. Buchanan and D.E. Honigs, *Advances in Near-Infrared Spectroscopy*, Spectroscopy **1**, 40-42 (1986).

15. R.A. Lodder, L. Cassis, and E.W. Ciurczak, *Arterial Analysis with a Novel Near-IR Fiber-Optic Probe*, Spectroscopy **5**, 12-16 (1990).

16. L.A. Cassis and R.A. Lodder, *Near-IR Imaging of Atheromas in Living Arterial Tissue*, in K.R. Billingsley, H.U. Brown, and E. Derohanes (eds.), *Scientific Excellence in Supercomputing: the 1990 IBM Contest Prize Papers*, Baldwin Press, Athens, 433-487 (1992).

17. C.V. Raman and K.S. Krishnan, *A New Type of Secondary Radiation*, Nature **121**, 501-502 (1928).

18. C.V. Raman, *A Change of Wave-length in Light Scattering*, Nature **121**, 619 (1928).

19. C.V. Raman and K.S. Krishnan, *The Optical Analogue of the Compton effect*, Nature **121**, 711 (1928).

20. D.A. Long, *Raman Spectroscopy*, McGraw-Hill, New York (1977).

21. G. Landsberg and L. Mandelstam, *Eine neue Erscheinung bei der Lichtzerstreuung in Krystallen*, Die Naturwissenschaften **16**, 557-558 (1928).

22. D.J. Gardiner and P.R. Graves (eds.), *Practical Raman Spectroscopy*, Springer-Verlag, Berlin (1989).

23. J.G. Grasselli, M. Snavely, and B.J. Bulkin, *Chemical Applications of Raman Spectroscopy*, Wiley, New York (1981).

24. J.G. Grasselli and B.J. Bulkin (eds.), *Analytical Raman Spectroscopy*, Wiley, New York (1991).

25. P.R. Carey, *Biochemical Applications of Raman and Resonance Raman Spectroscopies*, Academic Press, New York (1982).

40. M.J. Pelletier and R.C. Reeder, *Characterization of Holographic Band-Reject Filters Designed for Raman Spectroscopy*, Applied Spectroscopy **45**, 765-770 (1991).

41. C.L. Schoen, S.K. Sharma, C.E. Helsley, and H. Owen, *Performance of a Holographic Supernotch Filter*, Applied Spectroscopy **47**, 305-308 (1993).

42. H. Horinaka, N. Yamamoto, and H. Hamaguchi, *A New Approach to Highly Efficient Raman Spectroscopy Using a Laser Diode and $AgGaSe_2$ Crystal Filter*, Applied Spectroscopy **46**, 379-381 (1992).

43. A. Schulte, *Near-Infrared Raman Spectroscopy Using CCD Detection and a Semiconductor Bandgap Filter for Rayleigh Line Rejection*, Applied Spectroscopy **46**, 891-893 (1992).

44. R.J. Bell, *Introductory Fourier Transform Spectroscopy*, Academic Press, New York (1972).

45. S. Svanberg, *Atomic and Molecular Spectroscopy. Basic Aspects and Practical Applications*, Springer Verlag, Berlin (1991).

46. T. Hirschfeld and B. Chase, *FT-Raman Spectroscopy: Development and Justification*, Applied Spectroscopy **40**, 133-137 (1986).

47. H. Ishida, R. Kamoto, S. Uchida, A. Ishitani, Y. Ozaki, K. Iriyama, E. Tsukie, K. Shibata, F. Ishihara, and H. Kameda, *Raman Microprobe and Fourier Transform-Infrared Microsampling Studies of the Microstructrure of Gallstones*, Applied Spectroscopy **41**, 407-412 (1987).

48. S. Nie, K.L. Bergbauer, J.J. Ho, J.F.R. Kuck, N.-T Yu, *Applications of Near-Infrared Fourier Transform Raman Spectroscopy in Biology and Medicine*, Spectroscopy **5**, 24-32 (1990).

49. R.R. Alfano, C.H. Liu, W.L. Sha, H.R. Zhu, D.L. Akins, J. Cleary, R. Prudente, and E. Cellmer, *Human Breast Tissues Studied by IR Fourier Transform Raman Spectroscopy*, Lasers in Life Sciences **4**, 23-28 (1991).

50. Y. Ozaki, A. Mizuno, H. Sato, K, Kawauchi, and S. Muraishi, *Biomedical Application of Near-Infrared Fourier Transform Raman Spectroscopy. Part I: The l064-nm Excited Raman Spectra of Blood and Met Hemoglobin*, Applied Spectroscopy **46**, 533-536 (1992).

51. J.J. Baraga, M.S. Feld, and R.P. Rava, *In Situ Optical Histochemistry of Human Artery Using Near Infrared Fourier Transform Raman Spectroscopy*, Proceedings of the National Academy of Sciences of the USA **89**, 3473-3477 (1992).

52. R. Manoharan, J.J. Baraga, M.S. Feld, and R.P. Rava, *Quantitative Histochemical Analysis of Human Artery Using Raman Spectroscopy*, Journal of Photochemistry and Photobiology B: Biology **16**, 211-233 (1992).

26. R.H. Clarke, E.B. Hanlon, J.M. Isner, and H. Brody, *Laser Raman Spectroscopy of Calcified Atherosclerotic Lesions in Cardiovascular Tissue*, Applied Optics **26**, 3175-3177 (1987).

27. R.H. Clarke, Q. Wang, and J.M. Isner, *Laser Raman Spectroscopy of Atherosclerotic Lesions in Human Coronary Artery Segments*, Applied Optics **27**, 4799-4800 (1988).

28. V.R. Kodati and A.T. Tu, *Raman Spectroscopic Identification of Cysteine-Type Kidney Stone*, Applied Spectroscopy **44**, 837-839 (1990).

29. V.R. Kodati, A.T. Tu, and J.L. Turumin, *Raman Spectroscopic Identification of Uric-Acid-Type Kidney Stone*, Applied Spectroscopy **44**, 1134-1136 (1990).

30. S. Zheng and A.T. Tu, *Raman Spectroscopic Identification of Bilirubin-Type Gallstone*, Applied Spectroscopy **40**, 1099-1103 (1986).

31. S. Zheng and A.T. Tu, *Spectroscopic Identification of Gallstone*, Applied Spectroscopy **41**, 696-697 (1987).

32. A.T. Tu and S. Zheng, *Raman Spectroscopic Identification of Gallstones*, Vibrational Spectra and Structure **17A**, 485-496 (1989).

33. D.C.B. Redd, Z.C. Feng, K.T. Yue, and T.S. Gansler, *Raman Spectroscopic Characterisation of Human Breast Tissues: Implications for Breast Cancer Diagnosis*, Applied Spectroscopy **47**, 787-791 (1993).

34. A. Lauberau and M. Stockburger (eds.), *Time-Resolved Vibrational Spectroscopy*, Springer-Verlag, Berlin (1985).

35. T. Tahara and H.-O Hamaguchi, *Picosecond Raman Spectroscopy Using a Streak Camera*, Applied Spectroscopy **47**, 391-398 (1993).

36. J. Funfschilling and D.F. Williams, *CW Laser Wavelength Modulation in Raman and Site Selection Fluorescence Spectroscopy*, Applied Spectroscopy **30**, 443-446 (1976).

37. A.P. Shreve, N.J. Cherepy, and R.A. Mathies, *Effective Rejection of Fluorescence Interference in Raman Spectroscopy Using a Shifted Excitation Difference Technique*, Applied Spectroscopy **46**, 707-711 (1992).

38. S. Chadha, E. Ghiamati, R. Manoharan, and W. Nelson, *UV-Excited Raman and Resonance Raman Spectra of Synthetic Polymers*, Applied Spectroscopy **46**, 1176-1181 (1992).

39. M.M. Carrabba, K.M. Spencer, C. Rich, and D. Rauh, *The Utilization of a Holographic Bragg Diffraction Filter for Rayleigh Line Rejection in Raman Spectroscopy*, Applied Spectroscopy **44**, 1558-2562 (1990).

53. R.D. Billhorn, J.V. Sweedler, P.M. Epperson, and M.B. Denton, *Charge Transfer Device Detectors for Analytical Optical Spectroscopy - Operation and Characteristics*, Applied Spectroscopy **41**, 1114-1125 (1987).

54. J.M. Williamson, R.J. Bowling, and R.L. McCreery, *Near-Infrared Spectroscopy with a 783-nm Diode Laser and CCD Array Detector*, Applied Spectroscopy **43**, 372-375 (1989).

55. Y. Wang and R.L. McCreery, *Evaluation of a Diode Laser / Charge Coupled Device Spectrometer for Near-Infrared Raman Spectroscopy*, Analytical Chemistry **61**, 2647-2651 (1989).

56. C.D. Allred and R.L. McCreery, *Near-Infrared Raman Spectroscopy of Liquids and Solids with a Fiber-Optic Sampler, Diode Laser, and CCD Detectorer*, Applied Spectroscopy **44**, 1229-1231 (1990).

57. C.D. Newman, G.G. Bret, and R.L. McCreery, *Fiber-Optic Sampling Combined with an Imaging Spectrograph for Routine Raman Spectroscopy*, Applied Spectroscopy **46**, 262-265 (1992).

58. T.M. Niemczyk, M. Delgado-Lopez, and C.D. Newman, *Multichannel Raman Spectroscopy Tackles Industrial Problems*, Laser Focus World, 85-98 (November 1993).

59. J.J. Baraga, M.S. Feld, and R.P. Rava, *Rapid Near-Infrared Raman Spectroscopy of Human Tissue with a Spectrograph and CCD Detector*, Applied Spectroscopy **46**, 187-190 (1992).

60. D.D. Klug, D.L. Singleton, and V.M. Walley, *Laser Raman Spectrum of Calcified Human Aorta*, Lasers in Surgery and Medicine **12**, 13-17 (1992).

61. Schrader, *Chemische Anwendungen der Raman-Spectroscopie*, Angewandte Chemie **85**, 925-950 (1973).

62. M.C. Tobin, *Laser Raman Spectroscopy*, Wiley, New York (1971).

63. F.R. Dollish, W.G. Fateley, and F.F. Bentley, *Characteristic Raman Frequencies of Organic Compounds*, Wiley, New York (1974).

64. B. Schraeder, *Raman / Infrared Atlas of Organic Compounds* VCH Verlagsgesellschaft, Weinheim (1989).

65. Y. Nishimura, A.Y. Mirakawa, and M. Tsuboi, *Resonance Raman Studies of Nucleic Acids*, Advances in Infrared and Raman Spectroscopy **5**, 217-275 (1978).

66. G. Lindop, *Blood Vessels and Lymphatics*, in J.R. Andersson (ed.), *Muir's Textbook of Pathology*, Edward Arnold, London, 14.1-14.14 (1985).

67. S. Andersson-Engels, J. Johansson, K. Svanberg, and S. Svanberg, *Fluorescence Diagnosis and Photochemical Treatment of Diseased Tissue Using Lasers : Part II*, Analytical Chemistry **62**, 19A-27A (1990).

68. B. Masterson and J.Webb, *Better Diode Lasers Will Expand Applications in Many Key Areas*, Photonics Spectra, 119-124 (May 1992).

69. *270M Imaging Spectrograph with G.M.I. Software. Operation and Maintenance Instructions*, Spex Industries, Edison (1992).

8. Appendices

A. Basic units

The following relations are commonly used in atomic and molecular spectroscopy:

$$\text{Energy} = \Delta E = h\nu \tag{A.1}$$

$$\text{Wavelength} = \lambda = c/\nu \tag{A.2}$$

$$\text{Wavenumber} = 1/\lambda = \nu/c \tag{A.3}$$

$$\text{Frequency} = \nu = c/\lambda \tag{A.4}$$

where h is Planck's constant and c is the velocity of light. Using these relationships it is possible to express an energy interval in eV (energy), nm (=10^{-9} m, wavelength), cm^{-1} (wavenumber) or Hz (frequency). Table A.2 gives conversion factors between different units.

Table A.1 *Conversion factors between different energy units.*

Unit	Joule	cm^{-1}	Hz	eV
1 Joule	1	$5.03378 \cdot 10^{22}$	$1.50919 \cdot 10^{33}$	$6.24150 \cdot 10^{18}$
1 cm^{-1}	$1.98658 \cdot 10^{-23}$	1	$2.99792 \cdot 10^{10}$	$1.23992 \cdot 10^{-4}$
1 Hz	$6.62608 \cdot 10^{-34}$	$3.33565 \cdot 10^{-11}$	1	$4.12567 \cdot 10^{-15}$
1 eV	$1.60218 \cdot 10^{-19}$	$8.06502 \cdot 10^{3}$	$2.41799 \cdot 10^{14}$	1

The frequency is an inconveniently large number in the spectral range that are of interest in atomic and molecular spectroscopy and the wavenumber which is linear with both frequency and energy is more commonly used, but also wavelength that are inversely proportional to frequency and energy is widely used. In fluorescence spectroscopy the wavelength is the preferred unit, while in IR spectroscopy both wavenumber and wavelength are being used, with preference to wavenumber. The ultraviolet, visible, infrared, and microwave regions of the electromagnetic spectrum assumes the values shown in Table A.2.

In Raman spectroscopy, only the wavenumber is used and is largely due to historical accounts, but it is also for practical reasons. In a Raman spectrum the abscissa scale is always expressed in wavenumbers relative to the excitation wavenumber. If we excite a Raman spectra using 514.5 nm laser light and we observe a Raman peak at 542.4 nm, then the relative wavenumber shift is 1000 cm^{-1} (= 1/(514.5 nm) – 1/(542.5 nm). This peak is the Stokes component, the anti-Stokes component will be observed at 489.3 nm, i.e. at -1000 cm^{-1}. If we change the excitation wavelength to 1064 nm, we will observe a Raman peak at 1191 nm. This is the same peak as for 514.5 nm excitation ((1/(1064 nm) – 1/(1191 nm) = 1000 cm^{-1}). The wavelength difference changes from $\Delta\lambda$ = 28 nm to $\Delta\lambda$ = 127 nm, but the wavenumber shift (the energy associated with this vibrational

mode) is always the same.

Table A.2 *Values of wavelength, wavenumber, energy, and frequency of different regions of the electromagnetic spectrum.*

Region	Wavelength (m)	Wavenumber (cm^{-1})	Energy (eV)	Frequency (Hz)
Ultraviolet				
far	$1\cdot10^{-8}$ - $2\cdot10^{-7}$	$1\cdot10^{6}$ - 50000	125 - 6.2	$3\cdot10^{16}$ - $1.5\cdot10^{15}$
near	$2\cdot10^{-7}$ - $3.8\cdot10^{-7}$	50000 - 26300	6.2 - 3.2	$1.5\cdot10^{15}$- $7.9\cdot10^{14}$
Visible	$3.8\cdot10^{-7}$ - $7.8\cdot10^{-7}$	26300 - 12800	3.2- 1.6	$7.9\cdot10^{14}$ - $3.8\cdot10^{14}$
Infrared				
near	$7.8\cdot10^{-7}$ - $2.5\cdot10^{-6}$	12800 - 4000	1.6 - 0.5	$3.8\cdot10^{14}$ - $1.2\cdot10^{14}$
middle	$2.5\cdot10^{-6}$ - $5\cdot10^{-5}$	4000 - 200	0.5 - 0.02	$1.2\cdot10^{14}$ - $6\cdot10^{12}$
far	$5\cdot10^{-5}$ - $1\cdot10^{-3}$	200 - 10	0.02 - 0.001	$6\cdot10^{12}$ - $3\cdot10^{11}$
Microwave	$1\cdot10^{-3}$ - 1	10 - 0.01	$1\cdot10^{-3}$ - $1\cdot10^{-6}$	$3\cdot10^{12}$ - $3\cdot10^{8}$

B. Fourier transform spectroscopy

FT spectroscopy often uses an dual-beam interferometer of the Michelson type, as shown in Figs. B.1 and 2.6. With equal lengths of the two arms in the interferometer the path difference between the two interfering beams is zero. If the moving mirror is moved $\Delta/2$ a path difference of Δ is introduced (the beams go back and forth). If the light source emits monochromatic radiation and the beams are of equal intensity the intensity at the detector becomes

$$I(\Delta) = I_0 \cos^2 \phi \tag{B.1}$$

where

$$\phi = \pi \frac{\Delta}{\lambda} = \pi \nu \frac{\Delta}{c}. \tag{B.2}$$

If the light source instead emits a spectrum $B(\nu)$, the intensity at the detector becomes

$$I(\Delta) = \int_0^\infty B(\nu)\cos^2\left(\pi\nu\frac{\Delta}{c}\right)d\nu = \frac{1}{2}\int_0^\infty B(\nu)\left(1+\cos\left(2\pi\nu\frac{\Delta}{c}\right)\right)d\nu$$

$$= \frac{1}{2}\int_0^\infty B(\nu)d\nu + \frac{1}{2}\int_0^\infty B(\nu)\cos\left(2\pi\nu\frac{\Delta}{c}\right)d\nu = K + J(\Delta). \tag{B.3}$$

$J(\Delta)$ is called the interferogram and the spectrum $B(\nu)$ (which is recorded directly with a multichannel detector and a spectrometer) can be calculated from $J(\Delta)$ with the help

of the Fourier Transform

$$B(\nu) \propto \int_0^{\infty} J(\Delta)\cos\left(2\pi\nu\frac{\Delta}{c}\right)d\Delta. \tag{B.4}$$

One immediately realises that the integration cannot be performed from 0 to ∞ as the movable mirror can only be moved a limited distance and therefore the integration is performed over an finite interval. The Fourier Transform calculation is usually performed on a computer and very fast methods and algorithms have been constructed for that purpose. As can be seen in Fig. 2.6 there is a HeNe laser in Fourier Transform spectroscopy, and this laser is used to control the movements of the moveable mirror. (Further information and a detailed description of Fourier Transform spectroscopy can be found in Ref. [44].)

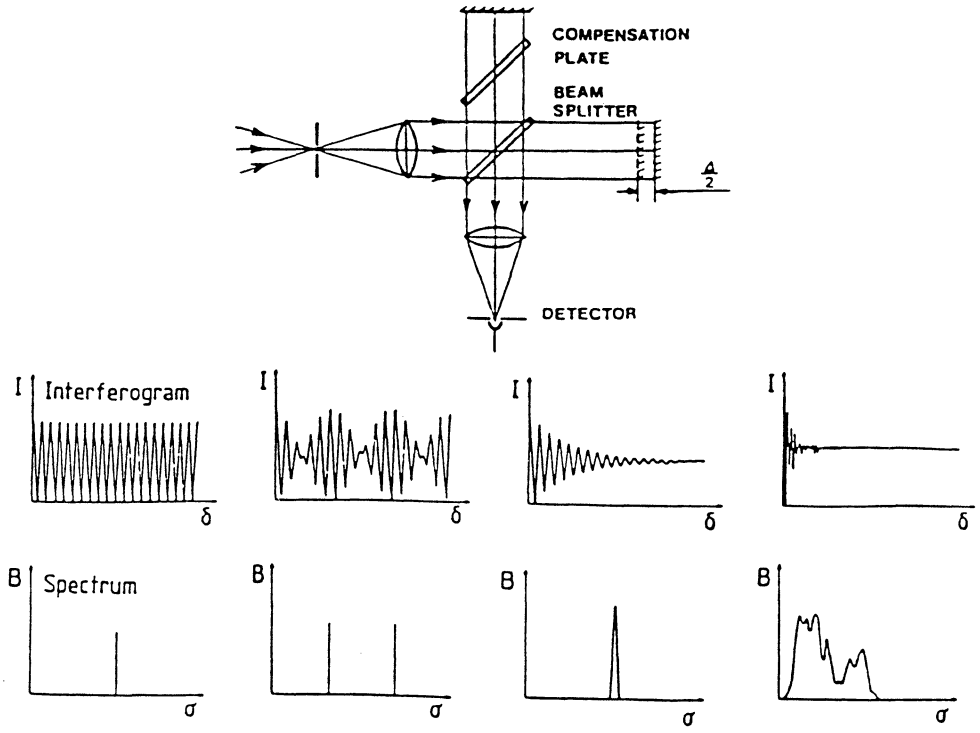

Fig. B.1 *FT spectrometer and basic signals. (From Ref. [45].)*

C. Characteristic wavenumbers and Raman Intensities of groups in organic compounds

(From Ref.[61].)

Vibration[a]	Region (cm^{-1})	Intensity[b]
ν(O-H)	3650 - 3000	w
ν(N-H)	3500 - 3300	m
ν(≡C-H)	3300	w
ν(=C-H)	3100 - 3000	s
ν(-C-H)	3000 - 2800	s
ν(-S-H)	2600 - 2550	s
ν(C≡N)	2255 - 2220	m - s
ν(C≡C)	2250 - 2100	vs
ν(C=O)	1820 - 1680	s - w
ν(C=C)	1900 - 1500	vs - m
ν(C=N)	1680 - 1610	s
ν(N=N), aliphatic substituent	1580 - 1550	m
ν(N=N), aromatic substituent	1440 - 1410	m
ν_a((C-)NO_2)	1590 - 1530	m
ν_s((C-)NO_2)	1380 - 1349	vs
ν_a((C-)SO_2(-C))	1340 - 1310	w - 0
ν_s((C-)SO_2(-C))	1160 - 1120	s
ν((C-)SO(-C))	1070 - 1020	m
ν(C=S)	1250 - 1000	s
δ(CH_2), δ_a(CH_3)	1470 - 1400	m
δ_s(CH_3)	1380	m - w s if at C=C
ν(CC), aromatics	1600, 1580	s - m
	1500, 1450	m - w
	1000	s (in mono-; m-; 1,3,5-derivatives)
ν(CC), alicyclics and aliphatic chains	1300 - 600	s - m
ν_a(C-O-C)	1150 - 1060	w
ν_s(C-O-C)	970 - 800	s - m
ν_a(Si-O-Si)	1110 - 1000	w - 0
ν_s(Si-O-Si)	550 - 450	vs
ν(O-O)	900 - 845	s
ν(S-S)	550 - 430	s
ν(Se-Se)	330 - 290	s
ν(C(aromatic)-S)	1100 - 1080	s
ν(C(aliphatic)-S)	790 - 630	s
ν(C-Cl)	800 - 550	s
ν(C-Br)	700 - 500	s
ν(C-I)	600 - 480	s
δ_s(CC), aliphatic chains		
C_n, n = 3, ..., 12	400 - 250	s - m
n>12	2495/n	
Lattice vibrations in molecular crystals (liberations and translational vibrations)	200 - 20	vs - 0

[a] ν, stretching vibrations; δ, bending vibrations; index s, symmetric; index a, antisymmetric.

[b] vs, very strong; s, strong; m, medium; w, weak; 0, very weak or inactive.

D. Observations about the spectrometer and CCD

An interesting but not so amusing effect was observed during this project, as unwanted peaks, "rubbish", is seen in the Raman spectra if the laser line is not attenuated enough. In this case, enough means $10^{-4} - 10^{-5}$. It was first observed when identical Raman spectra were recorded for the two solvents, 1,4-dioxane and toluene. As this hardly could be right, I begun to wonder what was wrong. I recorded a "pure" laser spectrum for both the 150 g/mm and 1200 g/mm gratings and "found" the answer, Fig. C.1 and Fig. C.2. Approximately 2-3 mm (the CCD is 9.7 x 9.7 mm) next to the laser line there are two broad unwanted peaks, and always on the Stokes side, never on the Anti-Stokes side.

Here are some of the observations I made:

A1. The location of the unwanted peaks are independent of the spectrometer grating. The peaks are always on the *same* spot on the CCD.
A2. If the gratings are rotated, i.e. scanning the spectrum, the unwanted peaks follow the laser line.
A3. Changing to a different laser (another diode laser at 840 nm and a HeNe-laser at 632 nm) only slightly alters the unwanted peaks.
A4. Trying in zero and second order of the spectrometer also only slightly alters the unwanted peaks.
A5. Testing with the laboratory background light does not give any results - the background is to high. In zero order and accumulation mode (i.e. to accumulate, sum, a number of spectra) one can faintly see the unwanted peaks with the 1200 g/mm grating.
A6. Decreasing the exposure time and running in accumulation mode only has a minor effect.

Following is a list of all the "experiments" I performed in order to get rid of the unwanted peaks but without any significant improvements:

B1. Removing as many reflections as possible *inside* the spectrometer by placing a lot of black paper beside, above, under and even partially over the mirrors and the gratings.
B2. Covering the CCD, or actually the material around it, by first placing black paper with a small hole both 1 cm and 10 cm in front of the CCD and then placing a cornet with a 1 cm x 1 cm hole facing the CCD and a 5 cm x 5 cm hole facing the last mirror of the spectrometer.
B3. Tilting (up to almost 1 cm) the CCD up and down, side to side, and also scanning the laser spectra with a small entrance hole (2mm x 10mm) to the CCD to determine if the extra peak originated from reflections from the CCD itself.
B4. Collimating and focusing the lens.
B5. Trying different angles of the incident light (in relation to the entrance slit of the spectrometer).
B6. Removing the spectrometer entrance slit cover, opening the entrance slit 5 cm and placing a rectangular (6 mm x 100 μm) fibre optic bundle *through* the entrance slit.
B7. Setting the CCD in sidelooking 90° rotation (i.e. just rotating the CCD 90°).
B8. Turning the spectrometer up-side down.

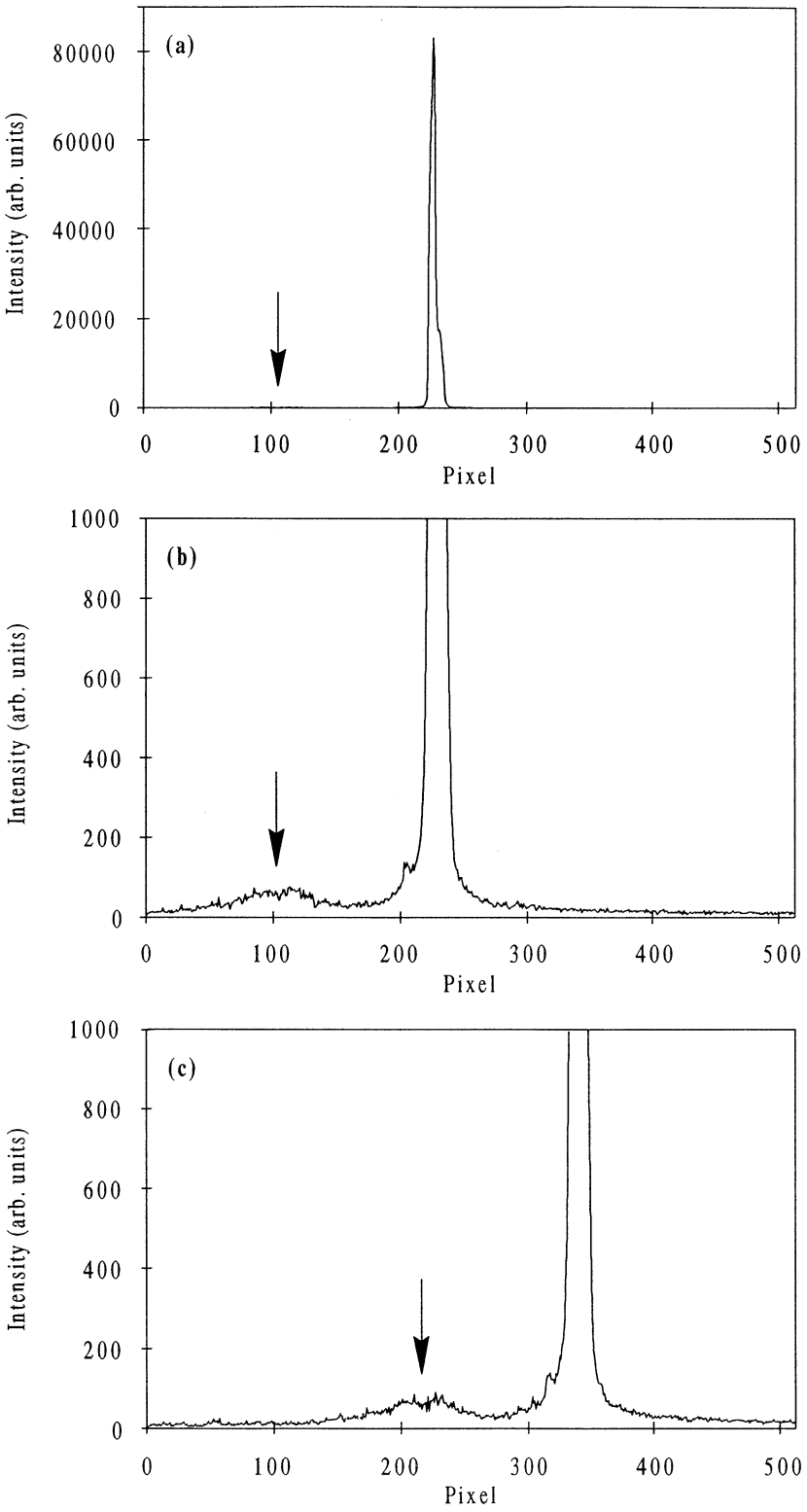

Fig. C.1 *Diode laser spectra with the 150 g/mm grating (a, b and c). (b) is a magnification of (a) and in (c) the grating has been set to another wavelength position. The arrows indicate the position of the unwanted peaks. The relation between the laser line and the unwanted peaks are approximately* $1:1 \cdot 10^{-3}$.

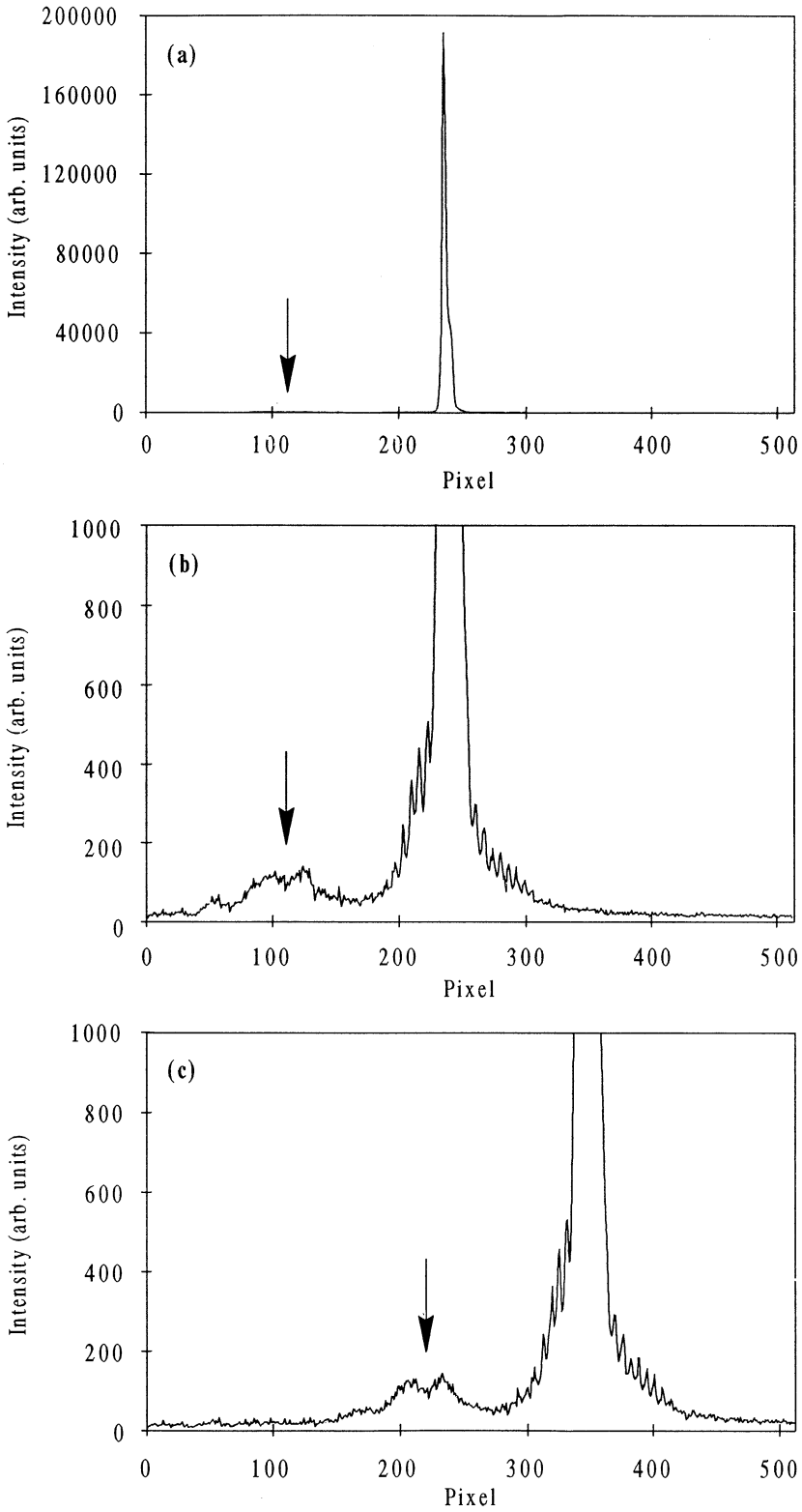

Fig. C.2 *Diode laser spectra with the 1200 g/mm grating (a, b and c). (b) is a magnification of (a) and in (c) the grating has been set to another wavelength position. The arrows indicate the position of the unwanted peaks. The relation between the laser line and the unwanted peaks are approximately 1:1·10^{-4}. The mode structure of the diode laser is seen as a ripple at the base of the laser line (b, c).*

From all these observations it is feasible to conclude that the unwanted peaks probably are rediffracted light and originate from the spectrometer (for instance B3 showed that it could not originate from the CCD).

Spex industries claims in their "Operation and Maintenance Instructions" [69] that; "Optical performance is radically improved over earlier designs by an unique Czerny-Turner configuration utilizing a proprietary aspheric optical correction. The optical correction provides for exceptional imaging capabilities. Astigmatism, inherent in classical Czerny-Turner systems, is negligible. The fast (f/4) system delivers near perfect spectral imaging over an area 25 mm wide by 12 mm high in the spectrograph image plane. The computer aided geometric design prevents rediffracted light from reaching the detector. With other designs this rediffracted light can be detected as an spurious signal."

In reality (in my experiments!) the computer aided design *does not* prevent *all* rediffracted light from reaching the detector. In fluorescence spectroscopy for instance this is no problem, as the measured signals are much stronger than the rediffracted light. In Raman spectroscopy on the other hand, where the signals are of the same magnitude or even smaller than the rediffracted light one can encounter serious problems if the laser line is not attenuated at least 10^{-4} times.

It is evident that if one wants to prevent rediffracted light from reaching the detector in Raman spectroscopy an excellent Rayleigh line rejection filter is essential, and without such a filter there is no hope of ever succeding with any Raman spectroscopy experiment with a Spex model 270M or other single spectrometers - equivalent effects was seen with another type of single-stage spectrometer, the PARC 1235.